

Responses to comments

Reviewer #1 (Astrid Blom)

1. Based on the authors' response to my previous 2nd comment I now understand what the authors mean by a flux based approach and an entrainment based approach. The authors' response is:

“We have now specifically defined what we mean by the flux form and entrainment form. See Lines 23-24 of the manuscript with track changes. We define again here: “Here we identify the flux form as based on the local capacity sediment transport rate, and the entrainment form as based on the local capacity entrainment rate”. Although we do not go into details in the paper, we note here that our system (the Yellow River) is suspension-dominated to the point where bedload is negligible. The phenomenon documented by Bell and Sutherland (1983) can be quantified using an entrainment-based bedload formulation such as Pelosi and Parker (2014). We note here that El kadi Abderrezzak and Pacquier (2009) list the form $dQ_s/dx = (Q_{scap} - Q_s)/L_{ad}$. where L_{ad} is the adaptation length. This is nothing more and nothing less than an entrainment form, but one for which the guts of the adaptation length L_{ad} remain undefined. In our system L_{ad} is specifically given as $q_w/(v_{sr}0)$, where q_w is the water discharge per unit width and v_s is fall velocity.”

This response in the response letter helped me a lot, and I actually find it clearer than the explanation in the revised manuscript. I'd suggest incorporating the above lines in the manuscript text, also the part of Bell&Sutherland, Pelosi&Parker and El Kadi Abderrezzak.

In trying to understand the essential difference between the flux form and the entrainment form, it was the following sentence by the authors that made the difference to me: “Here we define the flux form as based on the local capacity sediment transport rate, and the entrainment form as based on the local capacity entrainment rate.” I'd stress that information at various points of the manuscript: abstract, conclusions and introduction. I indeed do find that sentence in the revised abstract, but I'd move it upward as it is quite an important remark that will help the reader understand the essential difference between the two forms.

We have moved the sentence upward in the abstract, as suggested by the reviewer. See Lines 20-21 of the manuscript with track changes. We have also stressed this sentence in the Conclusions and the Introduction. See Lines 57-59 and Lines 677-679 of the manuscript with track changes. We think that the response in the last response letter, as mentioned by the reviewer, actually has already been discussed in the third paragraph of the Introduction.

2. Ln 54-55. The fact that one of the two (sediment transport rate or entrainment rate) is related to flow hydraulics is not the essence of the difference between the two forms, right? The essence rather is your phrase “Here we define the flux form as based on the local capacity sediment transport rate, and the entrainment form as based on the local capacity entrainment rate.”

The text has been revised as suggested by the reviewer. See Lines 57-59 of the manuscript with track changes.

3. Ln 25-26, 44. I find the terms equilibrium and nonequilibrium still confusing. I now understand that your words “(non)equilibrium” relate to the “sediment transport rate”. Yet if you’d decide to relate the words “(non)equilibrium” to the “entrainment rate”, would you have to reverse the use of the 2 words?

We think that we have been clear and consistent: the flux form corresponds to the equilibrium form, and the entrainment form corresponds to the nonequilibrium form.

4. Also see my previous Comment 26. I’d add the information on the numerical schemes for solving the equation of conservation of sediment mass (in the section on the flux form as well as in the section describing the entrainment form) to the manuscript. I may have overlooked though.

Information on the numerical schemes for solving the equation of conservation of sediment mass has been added for both the flux form and the entrainment form of the Exner equation. See Lines 188-189 and Lines 235-237 of the manuscript with track changes.

5. Ln 152-153. “For all the governing equations in this paper, the flood time scale is implemented by introducing t_f into each time derivative.” I am not sure I understand the meaning of this information. I think it would be relevant to let the reader know explicitly which time coordinate, t or t_f , is indicated in the legends of your figures? For instance, see figure 8. Maybe also list this information in the captions?

We have rewritten the sentence to make this issue clearer. We also now state explicitly that “results we exhibit later in this paper are all cast in terms of actual time scale t ”. See Lines 148-152 of the manuscript with track changes.

6. Section 2.3. I think the reader will need some help in this section.

- Why not start off with listing the general entrainment form of the conservation equation of sediment mass, where the right-hand term of Eq.8 is equal to $D_s - E_s$?
- then step by step explain what D_s is and how it is modelled?
- then E_s ?
- the information on slide 8 of Chapter 4 of Gary’s E-book would definitely help here
- I’d add references to the section
- please also indicate it if an equation is newly introduced (and so no references exist)

We did not add a new equation here, but rather we added a sentence to explain the two terms on the right hand side of Eq. (8). One of the terms denotes the dimensional entrainment rate and the other denotes the dimensional deposition rate. We think that this explanation should be enough for the reader to understand. See Lines 197-199 of the manuscript with track changes.

7. Eq (9). I do not understand the background of this equation. Can you help me and the reader out here?

Information has been added here to explain the equation for dimensionless entrainment rate E .

The basic idea is that “sediment transport reaches its equilibrium state ($q_s = q_{se}$) when the sediment deposition rate and the sediment entrainment rate balance each other ($r_{\theta}C = E$)”. See Lines 205-214 of the manuscript with track changes.

8. Ln 211. Please explain to the reader what is the physical meaning of the “sediment transport” being at equilibrium. I guess that under these conditions the upward sediment flux due to turbulent eddies is equal to the downward sediment flux related to gravity or the fall velocity. So under conditions in which the “sediment transport” is at equilibrium we are dealing with the Rouse profile?

We have explained in the manuscript that the condition of sediment transport being at equilibrium corresponds to “ $q_s = q_{se}$ ”(i.e. the sediment transport rate equals the sediment transport capacity). See Line 209 of the manuscript with track changes.

9. Ln 674. Please note that the instabilities reported by Chavarrias et al (2018) do not have a numerical origin. They result from complex eigenvalues of the system of equations and do not result from the numerical solution procedure.

We have revised the manuscript to render it more accurate. See Lines 673-674 of the manuscript with track changes.

10. Ln 49. alternate → alternative?

The manuscript has been revised as suggested by the reviewer.

11. Ln 121. Reference to E&H consists of an unwanted “.”, I think. Something like this is also found in L65.

We appreciate the reviewer for the correction. The manuscript has been revised.

12. Ln 183. Not sure you like how the symbol turns out here.

We have rewritten the symbol as $f_i|_{z_b-L_a}$ so as to show the two layers of subscripts.

13. Ln 275. This text could use some more nuance. Indeed Blom et al (2016, GRL) apply the fractional form of E&H that was introduced by Van der Scheer et al (2002). Yet Blom et al (2017, JGR) propose a much more general power law load relation for mixed-size sediment (called “GR”, but inspired on the form of E&H) that is capable of including hiding effects. It is listed in Eq 19 in Blom et al (2017 JGR). I think that the reason for it to not be applicable to the LYR is that it has not been calibrated to the LYR data and we do not know suitable values of the constants in the GR load relation. I do not think the reason for it to not be applicable to the LYR is that it does not include hiding effects.

We have revised the text to make it more accurate. We now state that the Engelund-Hansen

equation for mixtures as implemented by Van der Scheer et al. (2002) and Blom et al. (2016, 2017) is not applicable to the LYR because it has not been calibrated to the LYR data. See Lines 282-284 of the manuscript with track changes.

14. Ln 281 and 305. Porosity value is listed twice.

The sentence which lists the porosity value for the second time has been deleted. See Line 313 of the manuscript with track changes.

Reviewer #3

1. My primary suggestion concerns the presentation of the results comparing the two forms of the Exner equation – i.e., the “delta” metric. I think it is fine and appropriate to calculate the relative difference of the different variables predicted by the two models, but I have a concern that as framed, the delta metric may over- or (especially) under-represent the relative difference between the two results. For example, $\Delta(z_b)$ is shown to be within about 4% after 0.2 years for the uniform sediment simulations. This will be highly sensitive to the choice of elevation datum used in the model; i.e., if the initial upstream bed elevation is 1000 m instead of 20 m, then the 2.3 vs. 3 m of scour observed would lead to a $\Delta(z_b)$ of about 0.07%! I recommend calculating the delta values with the deviation from the initial condition, rather than the final value, for both the elevation and other variables (grain size, sediment transport rate). If that were done, then the $\Delta(z_b)$ for the uniform case would be $(3-2.3)/3 = 23\%$, instead of 4%. Calculating results this way may change some of the story, but I suspect the overall message would remain the same.

We admit that the values of $\Delta(z_b)$ depend on the choice of elevation datum. However, such a problem does not exist for the values of $\Delta(q_s)$, $\Delta(D_{sg})$ and $\Delta(D_{lg})$. The referee suggests that we calculate the delta values with the deviatoric bed elevation ($\Delta(z_b)$) from the initial condition rather than bed elevation (z_b) itself. This leads to a new problem. If the flux form predicts a deviatoric elevation of 0 m (or a very small value as in the numerical model), whilst the entrainment form predict a deviatoric elevation of 0.01 m, then $\Delta(z_b)$ will be infinitely large. But the difference between the predictions of the two forms is actually quite small (0 m vs. 0.01 m). For this reason, we have not replaced $\Delta(z_b)$ with $\Delta(z_b)$ as suggested by the reviewer.

What we have done in the manuscript is as follows: (1) we state that the value of $\Delta(z_b)$ depends on the choice of elevation datum, and that the downstream bed elevation is fixed as 0 m in this paper; and (2) we state that the maximum values of $\Delta(z_b)$ are almost always realized at the upstream end, where the bed elevation nevertheless does not deviate far from the initial value of 20 m. See Lines 377-380 of the manuscript with track changes. We hope this helps the reader understand the difference in bed elevation predicted by the two forms of the Exner equation.

2. A major motivating question for this paper is which version of the Exner equation is appropriate. The authors provide some guidance, suggesting that the adaptation length scale of the sediment in the system should be an important consideration, and I think their reasoning is sound. Some additional comparison with actual data from the Lower Yellow River would be helpful as well though – Does the LYR show evidence of sorting waves, etc., which could provide additional

context or support for this argument?

We have consulted our coauthor, Yuanfeng Zhang, who is perhaps the foremost (in China and thus the world) expert on sediment transport in the Yellow River. He says that the adjustment of grain size distribution of the LYR is quite smooth in space and time. No abrupt change of grain size distribution has been observed in the LYR. This serves as an indirect evidence that there are no clear sorting waves in the LYR. We have stated this in the manuscript. See Lines 629-631 of the manuscript with track changes.

3. Line 20: “local function of bed shear stress” = although it is common to use bed shear stress to calculate sediment transport rates, it is not the only possibility (i.e., one could use velocity, stream power, etc.). Suggest being a bit more general, perhaps “sediment transport is a function of local hydraulic conditions” or something.

The manuscript has been revised as suggested by the reviewer. See Lines 21-22 of the manuscript with track changes.

4. Line 21: “equilibrium” – suggest clarifying that here you mean equilibrium with hydraulic conditions (as opposed to local sediment balance).

The manuscript has been revised as suggested by the reviewer.

5. Line 22: “identify” is a strange word here – maybe use “represent”?

The manuscript has been revised as suggested by the reviewer.

6. Line 27: should be noted in the abstract that you are using a one-dimensional morphodynamic model.

Information has been added to the abstract. See Line 31 of the manuscript with track changes.

7. Line 33: Related to the general comment above – it would benefit the abstract to have a statement about which version of the Exner equation is appropriate in what circumstances.

Information has been added to the abstract. See Lines 37-38 of the manuscript with track changes.

8. Line 43: see comment above about local bed shear stress (line 20).

The manuscript has been revised as suggested by the reviewer. See Lines 47-48 of the manuscript with track changes.

9. Line 50: “pioneering work *on* bedload transport”

The manuscript has been revised accordingly.

10. Line 166: “summer” should be “summed”

The manuscript has been revised accordingly. We appreciate the reviewer for the correction.

11. Line 195: “form” should be “from”.

The text has been rewritten accordingly.

12. Line 260: double period at the end of the sentence

The manuscript has been revised accordingly.

13. Line 263: Can you give some justification as to why a relation without a hiding function is not appropriate for the LYR?

We have revised the text as suggested by Reviewer #1. We now state that the Engelund-Hansen equation for mixtures as implemented by Van der Scheer et al. (2002), Blom et al. (2016, 2017) is not applicable to the LYR because it has not been calibrated to the LYR data. See Lines 282-284 of the manuscript with track changes.

14. Line 292: The porosity used in the modeling was already given in line 268.

We have deleted the sentence. Thanks for the correction.

15. Lines 377-379: I am not convinced you need to include these sentences – just state that the supplement looks at hydrographs.

The sentences have been deleted as suggested by the reviewer.

16. Line 119: presumably the grain-size distribution of the flux is also fixed?

As we state in Lines 415-419 of the manuscript with track changes, the grain size distribution of the sediment feed (i.e. flux at upstream end) is fixed. It is not fixed in other locations, but is free to adjust morphodynamically.

17. Line 390: 173.7 Mt/a – is this correct? Adding washload nearly doubles the sediment load? Also, this value is larger than the stated range of 89-126 Mt/a.

Naito et al. (accepted subject to revision) estimate that 45% of the suspended load of LYR is washload based on data at the Huayuankou gauging station. This number agrees well with Fig. 1c of our paper, in which washload (finer than 45 μm) make up about 40% of the suspended load for various gauging stations of the LYR.

18. Figures 6, 7, and 8: The vertical axes on the grain size graphs say the values are in mm, not um.

The vertical axes of Figures 6, 7 and 8 have been corrected. The vertical axes of Figure S5 and S6 in the supplementary information have also been corrected. Thank you!

Morphodynamic model of Lower Yellow River: flux or entrainment form for sediment mass conservation?

Chenge An¹, Andrew J. Moodie², Hongbo Ma², Xudong Fu¹, Yuanfeng Zhang³, Kensuke Naito⁴, Gary Parker⁵

¹Department of Hydraulic Engineering, State Key Laboratory of Hydrosience and Engineering, Tsinghua University, Beijing, China.

²Department of Earth, Environmental and Planetary Sciences, Rice University, Houston, TX, USA.

³Yellow River Institute of Hydraulic Research, Zhengzhou, Henan, China.

⁴Department of Civil and Environmental Engineering, Hydrosystems Laboratory, University of Illinois, Urbana-Champaign, IL, USA.

⁵Department of Civil and Environmental Engineering and Department of Geology, Hydrosystems Laboratory, University of Illinois, Urbana-Champaign, IL, USA.

Correspondence to: Chenge An (anchenge08@163.com) and Xudong Fu (xdfu@tsinghua.edu.cn)

Abstract. Sediment mass conservation is a key factor that constrains river morphodynamic processes. In most models of river morphodynamics, sediment mass conservation is described by the Exner equation, which may take various forms depending on the problem in question. One of the most widely used forms of the Exner equation is the flux-based formulation, in which the conservation of bed material is related to the streamwise gradient of the sediment transport rate. An alternative form of the Exner equation, however, is the entrainment-based formulation, in which the conservation of bed material is related to the difference between the entrainment rate of bed sediment into suspension and the deposition rate of suspended sediment onto the bed. ~~Here we represent the flux form in terms of as based on the local capacity sediment transport rate, and the entrainment form in terms of as based on the local capacity entrainment rate.~~ In the flux form, sediment transport is a ~~local~~ function of local hydraulic conditions~~bed shear stress~~. However, the entrainment form does not require this constraint: only the rate of entrainment into suspension is in local equilibrium with hydraulic conditions, and the sediment transport rate itself may lag in space and time behind the changing flow conditions. ~~Here we identify the flux form as based on the local capacity sediment transport rate, and the entrainment form as based on the local capacity entrainment rate.~~ In modeling the fine-grained Lower Yellow River, it is usual to treat sediment conservation in terms of an entrainment (nonequilibrium) form rather than a flux (equilibrium) form, in consideration of the condition that fine-grained sediment may be entrained at one place but deposit only at some distant location downstream. However, the differences in prediction between the two formulations have not been comprehensively studied to date. Here we study this problem by comparing the results predicted by both the flux form and the entrainment form of the Exner equation, under conditions simplified from the Lower Yellow River (i.e. a significant reduction of sediment supply after the closure of the Xiaolangdi Dam). We use a one-dimensional morphodynamic model and sediment transport equations specifically adapted for the Lower Yellow River. We find that in a treatment of a 200 km reach using a single characteristic bed sediment size, there is little difference between the two forms since the corresponding adaptation

34 length is relatively small. However, a consideration of sediment mixtures shows that the two forms give very different patterns
35 of grain sorting: clear kinematic waves occur in the flux form but are diffused out in the entrainment form. Both numerical
36 simulation and mathematical analysis show that the morphodynamic processes predicted by the entrainment form are sensitive
37 to sediment fall velocity. We suggest that the entrainment form of the Exner equation might be required when the sorting
38 processes of fine-grained sediment is studied, especially when considering relatively short time scales.

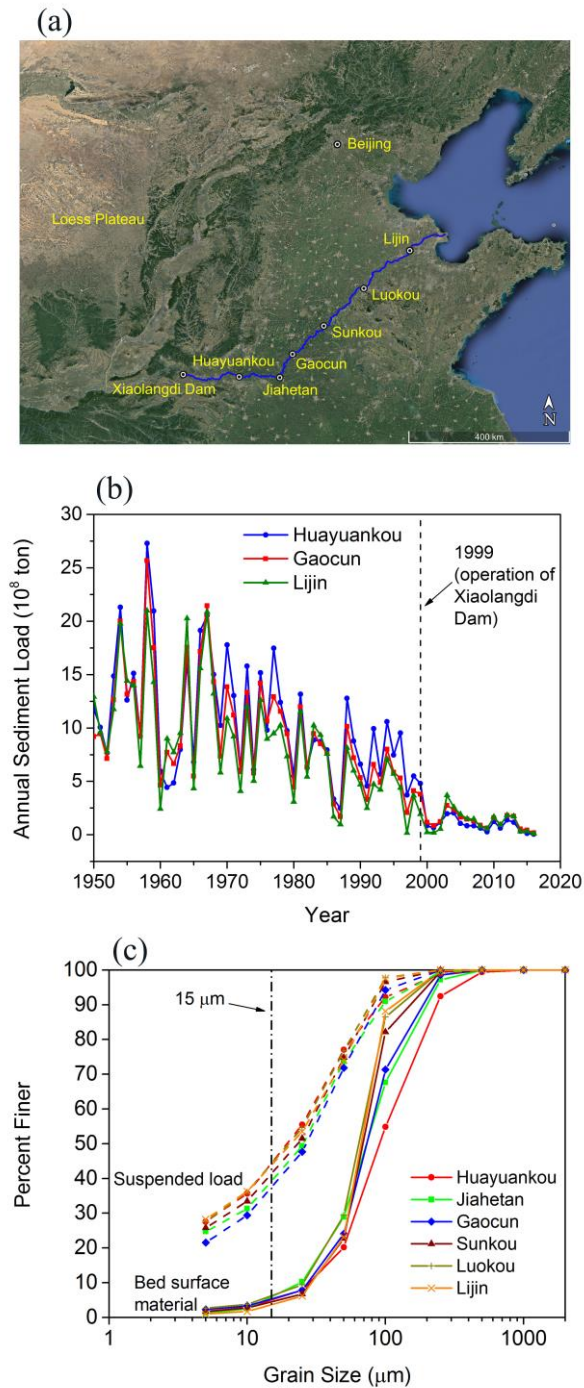
39 1. Introduction

40 Models of river morphodynamics often consist of three elements: (1) a treatment of flow hydraulics; (2) a formulation
41 relating sediment transport to flow hydraulics; and (3) a description of sediment conservation. In the case of unidirectional
42 river flow, the Exner equation of sediment conservation has usually been described in terms of a flux-based form in which
43 temporal bed elevation change is related to the streamwise gradient of the sediment transport rate. That is, bed elevation change
44 is related to $\partial q_s / \partial x$, where q_s is the total volumetric sediment transport rate per unit width and x is the streamwise coordinate
45 (Exner, 1920; Parker et al., 2004). This formulation is also referred to as the equilibrium formulation, since it considers
46 sediment transport to be at local equilibrium, i.e. q_s equals its sediment transport capacity q_{se} , as defined by the sediment
47 transport rate associated with local ~~bed shear stress~~ hydraulic conditions (e.g. bed shear stress, flow velocity, stream power,
48 etc.), regardless of the variation of flow conditions. Under this assumption, sediment transport relations developed under
49 equilibrium flow conditions (e.g., Meyer-Peter and Müller, 1948; Engelund and Hansen, 1967; Brownlie, 1981) can be
50 incorporated directly in such a formulation to calculate q_s , which is related to one or more flow parameters such as bed shear
51 stress.

52 An ~~alternate~~ alternative formulation, however, is available in terms of an entrainment-based form of the Exner
53 equation, in which bed elevation variation is related to the difference between the entrainment rate of bed sediment into the
54 flow and the deposition rate of sediment on the bed (Parker, 2004). The basic idea of the entrainment formulation can be traced
55 back to Einstein's (1937) pioneering work ~~of on~~ bedload transport, and has been developed since then by numerous researchers
56 so as to treat either bedload or suspended load (Tsujiimoto, 1978; Armanini and Di Silvio, 1988; Parker et al., 2000; Wu and
57 Wang, 2008; Guan et al., 2015). Such a formulation differs from the flux formulation in that the flux formulation is based on
58 the local capacity sediment transport rate whereas the entrainment formulation is based on the local capacity entrainment rate
59 into suspension, it is the rate of entrainment of bed sediment, rather than the sediment transport rate itself, that is related to flow
60 hydraulics. In the entrainment form, The difference between the local entrainment rate from the bed and the local deposition
61 rate onto the bed determines the rate of bed aggradation/degradation, and concomitantly the rate of loss/gain of sediment in
62 motion in the water column. Therefore, the sediment transport rate is no longer assumed to be in an equilibrium transport state,
63 but may exhibit lags in space and time after changing flow conditions. The entrainment formulation is also referred to as the
64 nonequilibrium formulation (Armanini and Di Silvio, 1988; Wu and Wang, 2008; Zhang et al., 2013).

65 To describe the lag effects between sediment transport and flow conditions, the concept of an adaptation length/time
66 is widely applied. This length/time characterizes the distance/time for sediment transport to reach its equilibrium state (i.e.,
67 transport capacity). Using the concept of the adaptation length, the entrainment form of the Exner equation can be recast into
68 a first-order “reaction” equation, in which the deformation term is related to the difference between the actual and equilibrium
69 sediment transport rates, as mediated by an adaptation length (which can also be recast as an adaptation time)- (Bell and
70 Sutherland, 1983; Armanini and Di Silvio, 1988; Wu and Wang, 2008; Minh Duc and Rodi, 2008; El kadi Abderrezzak and
71 Paquier, 2009). The adaptation length is thus an important parameter for bed evolution under nonequilibrium sediment
72 transport conditions, and various estimates have been proposed. For suspended load, the adaptation length is typically
73 calculated as a function of flow depth, flow velocity and sediment fall velocity (Armanini and Di Silvio, 1988; Wu et al., 2004;
74 Wu and Wang, 2008; Dorrell and Hogg, 2012; Zhang et al., 2013). The adaptation length of bedload, on the other hand, has
75 been related to a wide range of parameters, including the sediment grain size (Armanini and Di Silvio, 1988), the saltation step
76 length (Phillips and Sutherland, 1989), the dimensions of particle diffusivity (Bohorquez and Ancy, 2016), the length of dunes
77 (Wu et al., 2004), and the magnitude of a scour hole formed downstream of an inerodible reach (Bell and Sutherland, 1983).
78 For simplicity, the adaptation length can also be specified as a calibration parameter in river morphodynamic models (El kadi
79 Abderrezzak and Paquier, 2009; Zhang and Duan, 2011). Nonetheless, no comprehensive definition of adaptation length exists.

80 In this paper we apply the two forms of the Exner equation mentioned above to the Lower Yellow River (LYR) in
81 China. The LYR describes the river section between Tiexie and the river mouth, and has a total length of about 800 km. Figure
82 1(a) shows a sketch of the LYR along with 6 major gauging stations and the Xiaolangdi Dam, which is 26 km upstream of
83 Tiexie. The LYR has an exceptionally high sediment concentration (Ma et al., 2017), historically exporting more than 1 Gt of
84 sediment per year with only 49 billion tons of water, leading to a sediment concentration an order of magnitude higher than
85 most other large lowland rivers worldwide (Milliman and Meade, 1983; Ma et al., 2017; Naito et al., accepted subject to
86 revision). However, the LYR has seen a substantial reduction in its sediment load in recent decades, especially since the
87 operation of Xiaolangdi Dam in 1999 (Fig. 1(b)), because most of its sediment load is derived from the Loess Plateau which
88 is upstream of the reservoir (Wang et al., 2016; Naito et al., accepted subject to revision). Finally, the bed surface material of
89 the LYR is very fine, ranging as low as 15 μm . This is much finer than the conventional cutoff of washload (62.5 μm) employed
90 for sediment transport in most sand-bed rivers (National Research Council, 2007; Ma et al., 2017).



91
 92 **Figure 1.** (a) Sketch of Lower Yellow River, showing 6 major gauging stations and the Xiaolangdi Dam; (b) Annual sediment
 93 load of LYR measured at 3 gauging stations since 1950; (c) Grain size distributions of both bed surface material and suspended
 94 load measured at 6 gauging stations of the LYR.

95
96
97
98
99
100
101
102
103
104
105
106
107
108
109
110
111

112

113
114
115
116
117
118
119
120
121
122
123
124
125
126

When modeling the high-concentration and fine-grained LYR, it is common to treat sediment conservation in terms of an entrainment-based rather than a flux-based formulation. This is because many Chinese researchers view the entrainment formulation as more physically based, as it is capable of describing the behavior of fine-grained sediment, which when entrained at one place may be deposited at some distant location downstream (Zhang et al., 2001; Ni et al., 2004; Cao et al., 2006; He et al., 2012; Guo et al., 2008). However, the entrainment formulation is more computationally expensive and more complex to implement. In so far as the differences in prediction between the two formulations do not appear to have been studied in a systematic way, here we pose our central questions. Under what conditions is it valid to use the entrainment form of the Exner equation, and under what conditions may the flux form be used? Or more specifically, which form of the Exner equation is most suitable for the LYR?

Here we study this problem by comparing the results of flux-based and entrainment-based morphodynamics under conditions typical of the LYR. The organization of this paper is as follows. The numerical model is described in Section 2. In Section 3, the model is implemented to predict the morphodynamics of the LYR with a sudden reduction of sediment supply, which serves to mimic the effect of Xiaolangdi Dam. We find that the two forms of the Exner equation give similar predictions in the case of uniform sediment, but show different sorting patterns in the case of sediment mixtures. In Section 4, we conduct a mathematical analysis to explain the results in Section 3, and more specifically we quantify the effects of varied sediment fall velocity in the simulations. Finally, we summarize our conclusions in Section 5.

2. Model formulation

In this paper, we present a one-dimensional morphodynamic model for the Lower Yellow River. The fully unsteady Saint Venant Equations are implemented for the hydraulic calculation. Both the flux form and the entrainment form of the Exner equation are implemented in the model for sediment mass conservation. For each form of Exner equation, we consider both the cases of uniform sediment (bed material characterized by a single grain size) and sediment mixtures. Since the sediment is very fine in the LYR, the component of the load that is bedload is likely negligible (e.g. Ma et al., 2017), so that we consider only the transport of suspended load. Considering the fact that most accepted sediment transport relations (e.g., the Engelund and Hansen- (1967) relation) underpredict the sediment transport rate of the LYR by an order of magnitude or more (Ma et al., 2017), in our model we implement two recently developed generalized versions of the Engelund-Hansen relation which are based on data from the LYR. These are the version of Ma et al. (2017) for uniform sediment, and the version of Naito et al. (accepted subject to revision) for sediment mixtures. In cases considering sediment mixtures, we also implement the method of Viparelli et al. (2010) to store and access bed stratigraphy as the bed aggrades and degrades.

Since the aim of this paper is to compare the two formulations of the Exner equation in context of the LYR, rather than reproduce site-specific morphodynamic processes of the LYR, some additional simplifications are introduced to the model to facilitate comparison. The channel is simplified to be a constant-width rectangular channel, and bank (sidewall) effects and

127 floodplain interactions are not considered. The channel bed is assumed to be an infinitely deep supplier of erodible sediment
 128 with no exposed bedrock, which is justifiable because the LYR is fully alluvial, and has been aggrading for thousands of years,
 129 as copiously documented in Chinese history. Finally, water and sediment (of each grain size range) are fed into the upstream
 130 boundary at a specified rate, and at the downstream end of the channel we specify a fixed bed elevation along with a normal
 131 flow depth. These restrictions could be easily relaxed so as to incorporate site-specific complexities of the Yellow River.
 132 Because of the severe aggradation of the LYR developed before the Xiaolangdi Dam operation, the LYR is famous for its
 133 hanging bed (i.e. bed elevated well above the floodplain) and no major tributaries need be considered in the simulation.

134 2.1 Flow hydraulics

135 Flow hydraulics in a rectangular channel is described by the following 1D Saint Venant equations, which consider
 136 fluid mass and momentum conservation,

$$137 \frac{1}{I_f} \frac{\partial h}{\partial t} + \frac{\partial q_w}{\partial x} = 0 \quad (1)$$

$$138 \frac{1}{I_f} \frac{\partial q_w}{\partial t} + \frac{\partial}{\partial x} \left(\frac{q_w^2}{h} + \frac{1}{2} gh^2 \right) = ghS - C_f u^2 \quad (2)$$

$$139 C_f = C_z^{-2} \quad (3)$$

140 where t is time, h is water depth, q_w is flow discharge per unit width, g is gravitational acceleration, S is bed slope, u is depth-
 141 averaged flow velocity, C_f is dimensionless bed resistance coefficient, and C_z is the dimensionless Chezy resistance coefficient.
 142 In our model, the fully unsteady 1D Saint Venant equations are solved using a Godunov type scheme with the HLL (Harten-
 143 Lax-van Leer) approximate Riemann solver (Harten et al., 1983; Toro, 2001), which can effectively capture discontinuities in
 144 unsteady and nonuniform open channel flows.

145 In this paper, the full flood hydrograph of the LYR is replaced by a flood intermittency factor I_f (Paola et al., 1992;
 146 Parker, 2004). According to this definition, the river is assumed to be at low flow and not transporting significant amounts of
 147 sediment for time fraction $1 - I_f$; and is in flood at constant discharge and active morphodynamically for time fraction I_f . In the
 148 long term, the relation between the flood time scale t_f and the actual time scale t is $t_f = I_f t$. With the consideration that a river
 149 is in flood-occurs only for a fraction of time, here we introduce I_f into the time derivative of all governing equations, so that
 150 the flood time scale t_f is implemented in the simulation. For all the governing equations in this paper, the flood time scale is
 151 implemented by introducing I_f into each time derivative. This notwithstanding, the~~But~~ results we exhibit later in this paper are
 152 all cast in terms in the coordinate of actual time scale t . Full hydrographs are considered in the Supplement.

153 **2.2 Flux form of the Exner equation**

154 When dealing with uniform sediment, the flux form of the Exner equation can be written as,

155
$$\frac{1}{I_f} (1 - \lambda_p) \frac{\partial z_b}{\partial t} = - \frac{\partial q_s}{\partial x} \quad (4)$$

156 where λ_p is the porosity of the bed deposit, and z_b is bed elevation. Sediment transport is regarded to be in a quasi-equilibrium
 157 state, so that the sediment transport rate per unit width q_s equals the equilibrium (capacity) sediment transport rate per unit
 158 width q_{se} .

159 When considering sediment mixtures, an active layer formulation (Hirano, 1971; Parker, 2004) is incorporated in the
 160 flux-based Exner equation, so that the evolution of both bed elevation and surface grain size distribution can be considered. In
 161 this formulation, the river bed is divided into a well-mixed upper active layer and a lower substrate with vertical stratigraphic
 162 variations. The upper active layer therefore represents the volume of sediment that interacts directly with suspended load
 163 transport, and also exchanges with the substrate as the bed aggrades and degrades. Discretizing the grain size distribution into
 164 n ranges, the mass conservation relation for each grain size range can be written as,

165
$$\frac{1}{I_f} (1 - \lambda_p) \left[f_{ii} \frac{\partial}{\partial t} (z_b - L_a) + \frac{\partial}{\partial t} (F_i L_a) \right] = - \frac{\partial q_{si}}{\partial x} \quad (5)$$

166 where q_{si} is volumetric sediment transport rate per unit width of the i -th grain size range (taken to be equal to its equilibrium
 167 value q_{sei} in the flux formulation), F_i is the volumetric fraction of surface material in the i -th grain size range; f_{ii} is volumetric
 168 fraction of material in the i -th grain size range exchanged across the surface-substrate interface as the bed aggrades or degrades,
 169 and L_a is the thickness of active layer. For bedform-dominated sand-bed rivers, L_a is often related to the height of dunes (Blom,
 170 2008) so that the vertical sorting processes due to bedform migration can be considered. In this paper, a constant value of L_a
 171 is implemented in the simulation.

172 Summing Eq. (5) over all grain size ranges, one can find that the governing equation for bed elevation in case of
 173 sediment mixtures is the same as Eq. (4) upon replacing q_s with $q_{sT} = \Sigma q_{si}$, where q_{sT} denotes the total sediment transport rate
 174 per unit width ~~summer-summer~~ over all size ranges. Reducing Eq. (5) with Eq. (4) we get,

175
$$\frac{1}{I_f} (1 - \lambda_p) \left[L_a \frac{\partial F_i}{\partial t} + (F_i - f_{ii}) \frac{\partial L_a}{\partial t} \right] = f_{ii} \frac{\partial q_{sT}}{\partial x} - \frac{\partial q_{si}}{\partial x} \quad (6)$$

176 Therefore, in the flux formulation Eqs. (4) and (6) are implemented as governing equations for sediment mixtures,
 177 with Eq. (4) describing the evolution of bed elevation and Eq. (6) describing the evolution of surface grain size distribution.
 178 The exchange fractions f_{ii} between the active layer and the substrate are calculated using the following closure relation,

$$f_{ii} = \begin{cases} f_i|_{z_b-L_a} & \frac{\partial(z_b - L_a)}{\partial t} < 0 \\ \alpha F_i + (1-\alpha) p_{si} & \frac{\partial(z_b - L_a)}{\partial t} > 0 \end{cases} \quad (7)$$

That is, the substrate is transferred into the active layer during degradation, and a mixture of suspended load and active layer material is transferred into substrate during aggradation. In Eq. (7), $f_i|_{z_b-L_a}$ is the volumetric fraction of substrate material just beneath the interface, $p_{si} = q_{si}/q_{sT}$ is the fraction of bed material load in the i -th grain size range, and α is a specified parameter between 0 and 1. The formulation is adapted from Hoey and Ferguson (1994) and Toro-Escobar et al. (1996), who originally used it for bedload. In this paper, a value of 0.5 is specified for α .

The method of Viparelli et al. (2010) is applied in our model to store substrate stratigraphy and provide information for $f_i|_{z_b-L_a}$ (i.e., the topmost sublayer in Viparelli et al., 2010). The reader can refer to the original reference of Viparelli et al. (2010) for more details, or refer to An et al. (2017) for a concise description as to how to implement this method in a morphodynamic model. When solving the flux form of the Exner equation, a first-order upwinded scheme is implemented to discretize the spatial derivatives, and a first-order explicit scheme is implemented to discretize the temporal derivatives.

2.3 Entrainment form of the Exner equation

The entrainment-based Exner equation for uniform sediment is,

$$\frac{1}{I_f} (1 - \lambda_p) \frac{\partial z_b}{\partial t} = -v_s (E - r_0 C) \quad (8)$$

In Eq. (8), v_s is the fall velocity of sediment particles; E is the dimensionless entrainment rate of sediment normalized by sediment fall velocity; C is the depth-flux-averaged volume sediment concentration; and $r_0 = c_b/C$ is the recovery coefficient of suspended load which denotes the ratio between the near-bed sediment concentration c_b and the flux-averaged sediment concentration C . By definition, r_0 is related to the concentration profile of suspended load, and is expected to be no less than unity in cases appropriate for a depth-averaged shallow-water treatment of flow and morphodynamics. Therefore, the first term on the right hand side of Eq. (8), i.e. $v_s E$, denotes the sediment entrainment rate per unit area; the second term on the right hand side of Eq. (8), i.e. $v_s r_0 C$, denotes the sediment deposition rate per unit area.

For the sediment fall velocity v_s , we compare two widely used relations: the relation of Dietrich (1982), and the relation of Ferguson and Church (2004). Results show that these two relations give almost the same fall velocity for bed material load of the LYR, whose grain sizes typically fall in the range of 15 μm to 500 μm . Therefore, only the relation of

203 Dietrich (1982) is implemented in our simulations in this paper. Readers can refer to Section S1 of the Supplement for more
 204 details.

205 In the entrainment formulation the sediment transport rate q_s is not necessarily in its equilibrium state, but the
 206 dimensionless entrainment rate E is taken to be regarded to be at its capacity. The sediment transport rate q_s is calculated
 207 according to the following continuity relation,

$$208 \quad \underline{q_s = huC} \quad (9)$$

209 For the dimensionless entrainment rate E , we assume that sediment transport reaches its equilibrium state ($q_s = q_{se}$) when the
 210 sediment deposition rate and the sediment entrainment rate balance with each other ($r_0C = E$). Therefore, E can be back-
 211 calculated from q_{se} as,

212 ~~Since sediment transport is not necessarily in its equilibrium state in the entrainment formulation, we back-calculate~~
 213 ~~the sediment entrainment rate from the equilibrium sediment transport rate. Thus~~

$$214 \quad E = r_0 \frac{q_{se}}{q_w} \quad (910)$$

215 For the depth-flux-averaged sediment concentration C , another equation is implemented describing the conservation of
 216 suspended sediment in the water column,

$$217 \quad \frac{1}{I_f} \frac{\partial(hC)}{\partial t} + \frac{\partial(huC)}{\partial x} = v_s (E - r_0C) \quad (4011)$$

218 ~~Note that sediment transport is at equilibrium when $E = r_0C$. The sediment transport rate per unit width q_s obeys a continuity~~
 219 ~~relation,~~

$$220 \quad \underline{q_s = huC} \quad (11)$$

221 The entrainment-form Exner equation for sediment mixtures also uses the active layer formulation described in
 222 Section 2.2. Mass conservation of each grain size range can be written as,

$$223 \quad \frac{1}{I_f} (1 - \lambda_p) \left[f_{ii} \frac{\partial}{\partial t} (z_b - L_a) + \frac{\partial}{\partial t} (F_i L_a) \right] = -v_{si} (E_i - r_{0i} C_i) \quad (12)$$

$$224 \quad E_i = r_{0i} \frac{q_{sei}}{q_w} \quad (13)$$

225 where the subscript i denotes the i -th size range of sediment grain size.

Summing Eq. (12) over all grain size ranges, we get the governing equation for bed elevation,

$$\frac{1}{I_f} (1 - \lambda_p) \frac{\partial z_b}{\partial t} = - \sum_{j=1}^n v_{sj} (E_j - r_{0j} C_j) \quad (14)$$

Reducing Eq. (12) with Eq. (14) we get the governing equation for surface fraction F_i ,

$$\frac{1}{I_f} (1 - \lambda_p) \left[L_a \frac{\partial F_i}{\partial t} + (F_i - f_{li}) \frac{\partial L_a}{\partial t} \right] = f_{li} \sum_{j=1}^n v_{sj} (E_j - r_{0j} C_j) - v_{si} (E_i - r_{0i} C_i) \quad (15)$$

The governing equation for the sediment concentration of each grain size C_i can be written as,

$$\frac{1}{I_f} \frac{\partial (hC_i)}{\partial t} + \frac{\partial (huC_i)}{\partial x} = v_{si} (E_i - r_{0i} C_i) \quad (16)$$

and the sediment transport rate per unit width for the i -th size range q_{si} obeys the following continuity relation,

$$q_{si} = huC_i \quad (17)$$

In the entrainment formulation, the closure relation for f_{li} is the same as that used in the flux formulation (i.e., Eq. (7)), and the substrate stratigraphy is also stored and accessed using the method of Viparelli et al. (2010). When discretizing the entrainment form of the Exner equation, a first-order upwinded scheme is implemented for the spatial derivatives, and a first-order explicit scheme is implemented for the temporal derivatives.

2.4 Sediment transport relation

2.4.1 Uniform sediment

To close the Exner equations described in Sections 2.2 and 2.3, equations for equilibrium sediment transport rate q_{se} (q_{sei}) are still needed. For the simulations using uniform sediment, we implement the generalized Engelund-Hansen relation proposed by Ma et al. (2017). This equation is based on the data from LYR and can be written in the following dimensionless form,

$$q_s^* = \frac{\alpha_s}{C_f} (\tau^*)^{n_s} \quad (18)$$

where q_s^* is dimensionless sediment transport rate per unit width (i.e., the Einstein number), and τ^* is dimensionless shear stress (i.e., the Shields number). They are defined as,

$$247 \quad q_s^* = \frac{q_{se}}{\sqrt{RgDD}} \quad (19)$$

$$248 \quad \tau^* = \frac{\tau_b}{\rho RgD} \quad (20)$$

$$249 \quad \tau_b = \rho C_f u^2 \quad (21)$$

250 where D is the characteristic grain size of the bed sediment (here approximated as uniform); τ_b is bed shear stress; and R is
 251 submerged specific gravity of sediment, defined as $(\rho_s - \rho) / \rho$, in which ρ_s is density of sediment, and ρ is density of water.
 252 The sediment submerged specific gravity R is specified as 1.65 in this paper, which is an appropriate estimate for natural rivers,
 253 and corresponds to quartz.

254 In the relation of Ma et al. (2017), the dimensionless coefficient $\alpha_s = 0.9$ and the dimensionless exponent $n_s = 1.68$.
 255 These values are quite different from the original relation of Engelund and Hansen (1967), in which $\alpha_s = 0.05$ and $n_s = 2.5$.
 256 Ma et al. (2017) demonstrated that such differences imply that the riverbed of the LYR is dominated by low-amplitude bedform
 257 features (dunes) approaching upper-regime plane bed. According to this finding, form drag is then neglected in our modeling,
 258 and all of the bed shear stress is used for sediment transport.

259 **2.4.2 Sediment mixtures**

260 We implement the relation of Naito et al. (accepted subject to revision) to calculate the equilibrium sediment transport
 261 rate of size mixtures. Using field data from the LYR, Naito et al. (accepted subject to revision) extended the Engelund and
 262 Hansen (1967) relation to a surface-based grain-size specific form, in which the suspended load transport rate of the i -th size
 263 range is tied to the availability of this size range on the bed surface:

$$264 \quad q_{sei} = \frac{N_i^* F_i u_*^3}{RgC_f} \quad (22)$$

265 where N_i^* is the dimensionless sediment transport rate in the i -th size range, and u_* is shear velocity calculated from the bed
 266 shear stress τ_b :

$$267 \quad u_* = \sqrt{\frac{\tau_b}{\rho}} \quad (23)$$

268 The transport relation itself takes the form,

$$N_i^* = A_i \left(\tau_g^* \frac{D_{sg}}{D_i} \right)^{B_i} \quad (24)$$

in which D_i is the characteristic grain size for sediment in the i -th size range, D_{sg} is the geometric mean grain size in the active layer, and τ_g^* is the dimensionless bed shear stress associated with D_{sg} . The parameters τ_g^* , coefficient A_i , and exponent B_i are calculated as,

$$\tau_g^* = \frac{\tau_b}{\rho R g D_{sg}} \quad (25)$$

$$A_i = 0.46 \left(\frac{D_i}{D_{sg}} \right)^{-0.84} \quad (26)$$

$$B_i = 0.35 \left(\frac{D_i}{D_{sg}} \right)^{-1.16} \quad (27)$$

If A_i and B_i are specified as constant values in Eq (24), then the sediment transport rate for each size range depends only on the flow shear stress and the characteristic grain size of this size range, without being affected by other size ranges. But according to Eqs. (26) and (27), the coarser the sediment the smaller the values of A_i and B_i will be, thus leading to reduced mobility for coarse sediment (and increased mobility for fine sediment) due to the presence of grains of other sizes. Thus the relations (26) and (27) serve as hiding function that allow for grain sorting.

We note that a form of the Engelund-Hansen equation for mixtures was introduced by Van der Scheer et al. (2002), and implemented by Blom et al. (2016, 2017). Blom et al. (2017) further extended this relation to a more general framework which is capable of including hiding effects. These forms, however, have not been calibrated to the LYR data and are has no hiding formulation built into it, and is thus not suitable for the LYR.

3. Numerical modeling of the LYR using the two forms of Exner equation

In this section, we conduct numerical simulations using both the flux form and the entrainment form of the Exner equation, with the aim to study under what circumstances the two forms give different predictions. Numerical simulations are conducted in the setting of the LYR. We specify a 200 km long channel reach for our simulations, along with a constant channel width of 300 m and an initial longitudinal slope of 0.0001. Bed porosity λ_p is specified as 0.4. Based on field measurements of the LYR available to us, we implemented a dimensionless Chezy resistance coefficient C_z of 30, which corresponds to a dimensionless bed resistance coefficient C_f of 0.0011. For the entrainment form of Exner equation, we specify

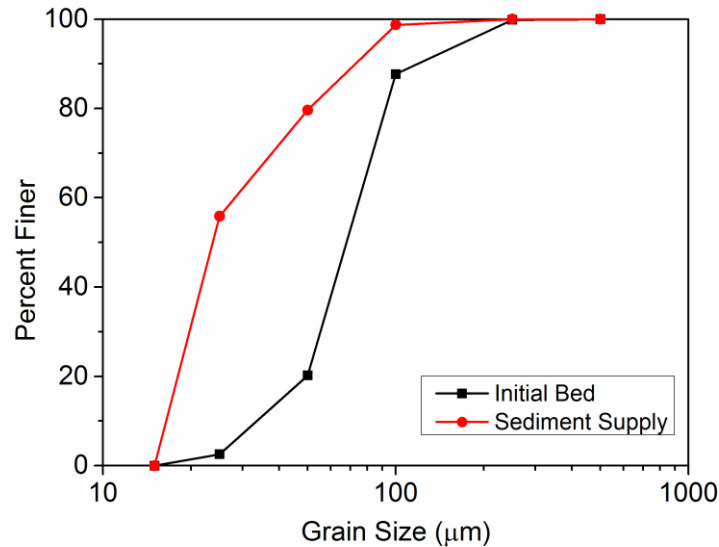
292 the ratio of near bed sediment concentration to flux-averaged sediment concentration r_0 (r_{0i}) = 1. Such a value of r_0 (r_{0i})
293 corresponds to a vertically uniform profile of sediment concentration, and will thus give a maximum difference between the
294 prediction of entrainment form and the prediction of the flux form. More discussion about the effects of r_0 is presented in
295 Section 4.3.

296 A constant flow discharge of 2000 m³/s (corresponding to a flow discharge per unit width q_w of 6.67 m²/s) is
297 introduced at the inlet of the channel with the flood intermittency factor I_f estimated as 0.14 (Naito et al., accepted subject to
298 revision). The downstream end is specified far from the river mouth to neglect the effects of backwater. Therefore, the bed
299 elevation is held constant and the water depth is specified as the normal flow depth at the downstream end of the calculational
300 domain. The above flow discharge per unit width q_w combined with the bed slope S as well as the bed resistance coefficient C_f
301 leads to a normal flow depth of 3.69 m. In our simulation, we use the height of bedforms in the LYR to determine the thickness
302 of the active layer (Blom, 2008). According to the field survey of Ma et al. (2017), the characteristic height of bedforms in the
303 LYR is about 20% of the normal flow depth, which can fall in the range suggested by the data analysis of Bradley and Venditti
304 (2017). This eventually leads to an estimate of active layer thickness of $L_a = 0.738$ m. The sublayer in the substrate to store the
305 vertical stratigraphy is specified with a thickness of 0.5 m.

306 Two cases are considered here. In the first case, the sediment grain size distribution of LYR is simplified to a uniform
307 grain size of 65 μm . This is based on the measured grain size distribution of bed material at the Lijin gauging station, which
308 has a median grain size of $D_{50} = 66.6$ μm , a geometric mean grain size of $D_g = 65.5$ μm , and a geometric standard deviation
309 $\sigma_g = 2.0$, as shown in Fig. 1(c). In the second case, we consider the effects of sediment mixtures. The grain size distribution of
310 the initial bed is based on the bed material at the Lijin gauging station, as shown in Fig. 1(c), but we renormalize the measured
311 grain size distribution with a cutoff for washload at 15 μm as suggested by Ma et al. (2017). The renormalized grain size
312 distribution for the initial bed as implemented in the case of sediment mixtures is shown in Fig. 2, with a total number of grain
313 size fractions of 5. ~~The sediment porosity λ_p is taken as 0.4 in this paper.~~ In both the two cases, simulations start with an
314 equilibrium state where sediment supply rate, sediment transport rate, and equilibrium sediment transport rate being the same,
315 so that the initial state of the channel is in equilibrium. Then we cut the sediment supply rate (of each size range) to only 10%
316 of the equilibrium sediment transport rate and keep this sediment supply rate. This is to mimic the reduction of sediment load
317 in the LYR in recent years, as shown in Fig. 1(b). The grain size distribution of sediment supply in the case of sediment
318 mixtures is shown in Fig. 2.

319 The 200 km channel reach is discretized into 401 cells, with cell size Δx of 500 m. In the case of uniform sediment,
320 we specify a time step for morphologic calculation $\Delta t_m = 10^{-4}$ year and a time step for hydraulic calculation $\Delta t_h = 10^{-6}$ year. In
321 the case of sediment mixtures, we specify a time step for morphologic calculation $\Delta t_m = 10^{-5}$ year, and a time step for hydraulic
322 calculation $\Delta t_h = 10^{-6}$ year. Computational conditions are briefly summarized in Table 1. The computational conditions we
323 implement are much simpler than the rather complicated conditions of the actual LYR. But it should be noted that the aim of

324 this paper is not to reproduce specific aspects of the morphodynamic processes of LYR, but to compare the flux form and
 325 entrainment form of Exner equation in the context of conditions typical of LYR.



326 **Figure 2.** Grain size distributions of both the initial bed and the sediment supply in the case of sediment mixtures. For the
 327 initial bed, the surface and substrate grain size distributions are the same. The grain size distribution of the initial bed is
 328 renormalized based on the field data at the Lijin gauging station. The grain size distribution of the sediment supply equals to
 329 the grain size distribution of bed material load at equilibrium. Grain sizes in the range of washload have been removed from
 330 both distributions.
 331

332 **Table 1.** Summary of computational conditions for numerical modeling of the LYR.

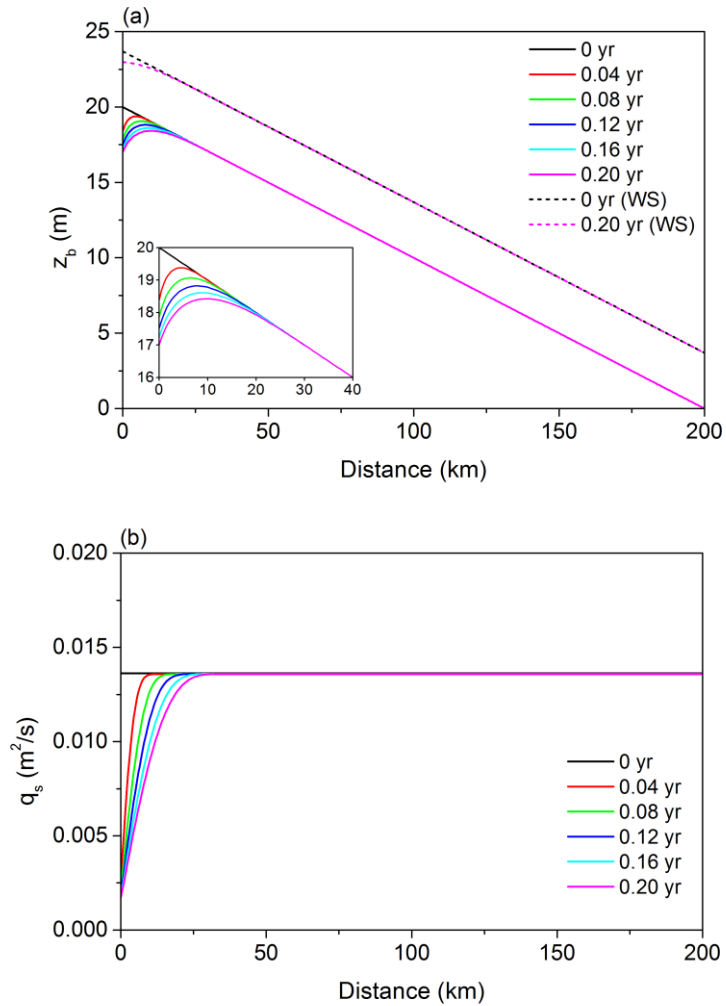
Parameter	Value
Channel length L	200 km
Channel width B	300 m
Initial slope S_f	0.0001
Dimensionless Chezy resistance coefficient C_z	30
Flow discharge per unit width q_w	6.67 m ² /s
Flood intermittency factor I_f	0.14
ratio of near bed concentration to average concentration r_0 (r_{0i})	1
Characteristic grain size in the case of uniform sediment	65 μm
Submerged specific gravity of sediment R	1.65
Porosity of bed deposits λ_p	0.4
cell size Δx	500 m
time step for morphologic calculation Δt_m	10 ⁻⁴ year (uniform sediment) 10 ⁻⁵ year (sediment mixtures)

333

334 **3.1 Case of uniform sediment**

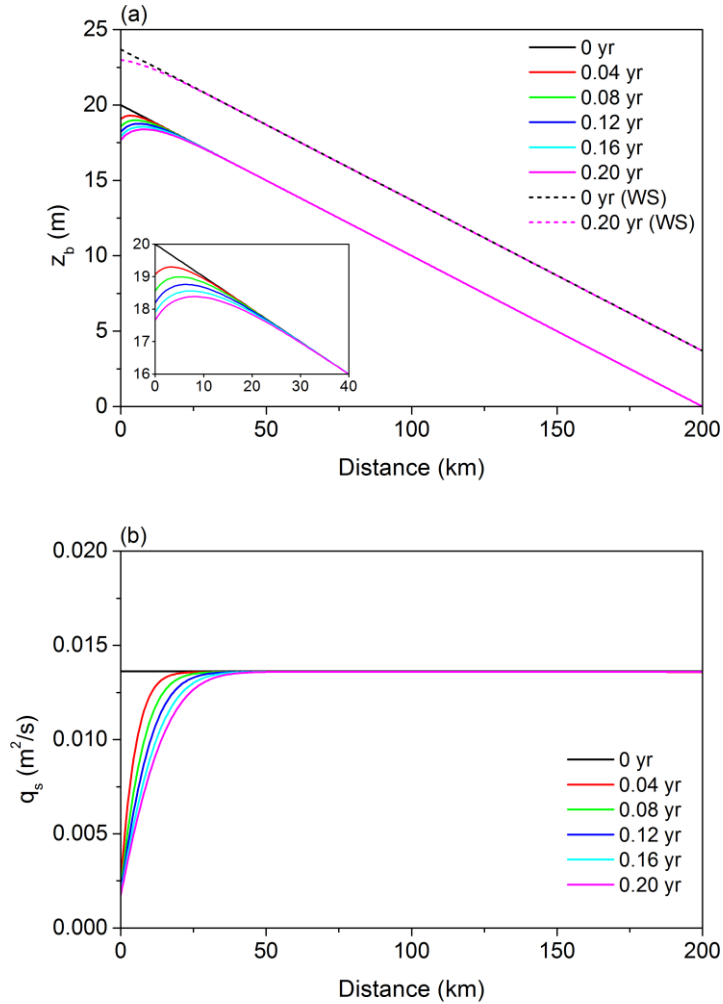
335 In this case, we implement a uniform grain size of 65 μm for both the bed material and sediment supply. Such a grain
336 size is nearly equal to the observed median grain size (or geometric mean grain size) of bed material at Lijin gauging station.
337 The relation of Ma et al. (2017) is implemented to calculate the transport rate of bed material suspended load. This relation
338 provides an equilibrium sediment transport rate per unit width q_{se} of 0.0136 m^2/s under the given flow discharge, bed slope
339 and sediment grain size. With a flood intermittency factor I_f of 0.14, this further gives a mean annual bed material load of 47.8
340 Mt/a. Adding in washload according to the estimate of Naito et al. (accepted subject to revision), total mean annual load is
341 86.9 Mt/a, a value that is of the same order of magnitude as averages over the period 2000-2016 (89-126 Mt/a depending on
342 site), i.e. since the operation of Xiaolangdi Dam in 1999 (Fig. 1(b)). The sediment supply rate q_{sf} we specify at the upstream
343 end of the channel is only 10% of the equilibrium sediment transport rate (i.e. sediment supply rate is cut by 90% from the
344 equilibrium state), such that $q_{sf} = 0.00136 \text{ m}^2/\text{s}$.

345 Figure 3 shows the modeling results using the flux form of the Exner equation. As we can see in the figure, the bed
346 degrades and the sediment load decreases in response to the cutoff of sediment supply. Such adjustments start from the
347 upstream end of the channel and gradually migrate downstream. Figure 4 shows the modeling results using the entrainment
348 form of Exner equation. A comparison between Fig. 4 and Fig. 3 shows that the entrainment form and the flux form give very
349 similar predictions in this case. The entrainment form provides a somewhat slower degradation (at the upstream end the flux
350 form predicts a 3-m degradation whereas the entrainment form predicts a 2.3-m degradation) and a more diffusive sediment
351 load reduction. Such more diffusive predictions of sediment load variation can be ascribed to the condition of nonequilibrium
352 transport that is embedded in the entrainment form. This issue will be studied analytically in Section 4. Here we present the
353 results for only 0.2 year after the cutoff of sediment supply, since the differences between the predictions of the two forms
354 tend to be the most evident shortly after the disruption but gradually diminish as the river approaches the new equilibrium (El
355 kadi Abderrezzak and Paquier, 2009). Modeling results over a longer time scale will be discussed in Section 4.3.



356
 357
 358
 359

Figure 3. 0.2 year results for the case of uniform sediment using the flux form of Exner equation: time variation of (a) bed elevation z_b and water surface (WS), (b) sediment load per unit width q_s of the LYR in response to the cutoff of sediment supply. The inset shows detailed results near the upstream end.



360
 361 **Figure 4.** 0.2 year results for the case of uniform sediment using the entrainment form of Exner equation: time variation of (a)
 362 bed elevation z_b and water surface (WS), (b) sediment load per unit width q_s of the LYR in response to the cutoff of sediment
 363 supply. The inset shows detailed results near the upstream end.

364 To further quantify the differences between the predictions of the two forms, we propose the following normalized
 365 parameter,

$$366 \quad \delta(y) = \left| \frac{y_E - y_F}{y_F} \right| \times 100\% \quad (28)$$

367 where y denotes an arbitrary variable calculated by the morphodynamic model, and subscripts F and E denote results using the
 368 flux form and the entrainment form respectively. Therefore, $\delta(y)$ denotes the difference between the prediction the two forms
 369 y_F and y_E normalized by the prediction of the flux form y_F .

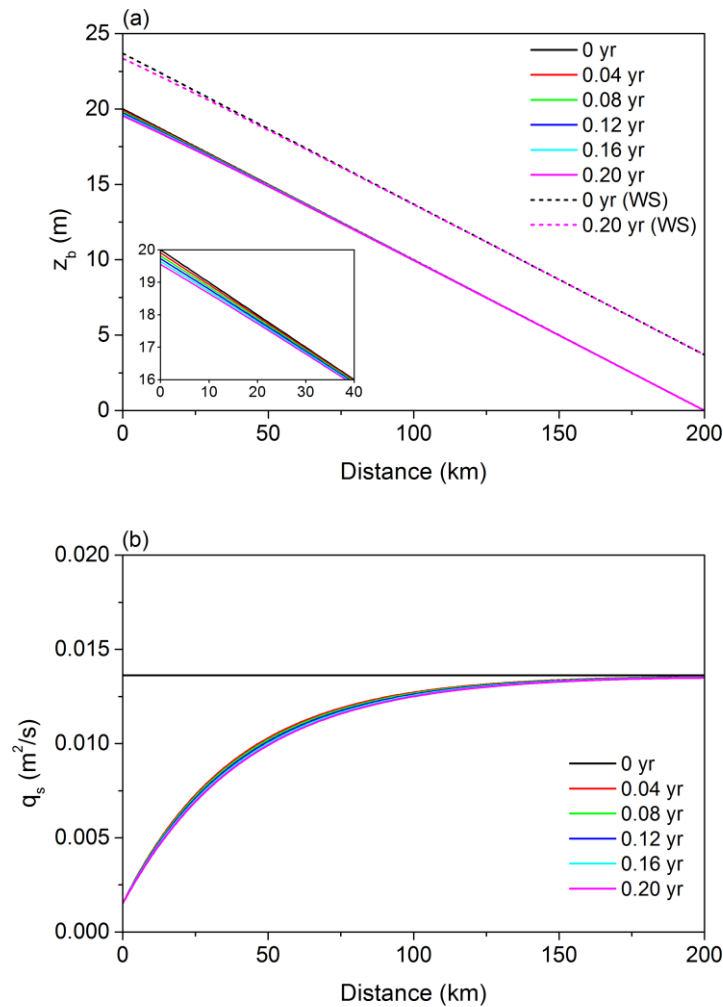
370 Table 2 gives a summary of the maximum values of δ along the channel at different times in the case of uniform
 371 sediment. The values of δ for both z_b and q_s are presented. As we can see from the table, the maximum value of $\delta(z_b)$ along the
 372 calculational domain stays within 4% in the first 0.2 year after the cutoff of sediment supply. This indicates that the flux form
 373 and the entrainment form can indeed give almost the same prediction in terms of bed elevation in this case. But in the case of
 374 the sediment load per unit width q_s , the maximum value of $\delta(q_s)$ can be as high as 20%, indicating that even though the two
 375 forms give qualitatively similar patterns of evolution in terms of sediment load as shown in Figs. 3 and 4, a quantitative
 376 difference is clearly evident due to the more diffusive nature of the predictions of the entrainment form. The value of $\delta(q_s)$ is
 377 largest at the beginning of the simulation, and then gradually reduces with time. It should be noted that the values of $\delta(z_b)$
 378 depend on the choice of elevation datum. In this paper bed elevation at the downstream end is fixed as 0 m, which serves as
 379 the elevation datum. In the simulation of this paper, the maximum value of $\delta(z_b)$ almost always occurs at the upstream end,
 380 where bed elevation deviates not too far from the initial value of 20 m.

381 **Table 2.** Quantification of the difference between predictions of the flux form and the entrainment form in the case of uniform
 382 sediment. The maximum values of $\delta(z_b)$ and $\delta(q_s)$ in the calculational domain are presented every 0.04 year.

		0.04 yr	0.08 yr	0.12 yr	0.16 yr	0.20 yr
original v_s	$\delta(z_b)$	3.7 %	3.9 %	3.9 %	3.9 %	3.8 %
	$\delta(q_s)$	20.5 %	15.1 %	12.3 %	10.5 %	9.2 %
v_s multiplied by 0.05	$\delta(z_b)$	8.2 %	10.9 %	12.7 %	13.9 %	14.9 %
	$\delta(q_s)$	74.8 %	68.1 %	63.0 %	58.9 %	55.4 %

383
 384 The above results show that the flux form and the entrainment form can provide similar predictions of LYR when the
 385 bed sediment grain size distribution is simplified to a uniform value of 65 μm . To understand under what conditions the two
 386 forms will lead to more different results, we conduct an idealized run using the entrainment form in which the sediment fall
 387 velocity v_s is arbitrarily multiplied by a factor of 0.05. That is to say, we keep the sediment grain size at 65 μm in the
 388 computation of the Shields number, but let the sediment fall velocity in Eqs. (8) and (10) equal only 1/20 of the value calculated
 389 by the relation of Dietrich (1982) from this grain size. With a much smaller, and indeed intentionally unrealistic sediment fall
 390 velocity, the entrainment form predicts very different results as shown in Fig. 5. The adjustment of the sediment load become
 391 even more diffusive in space: it takes almost the entire 200 km reach for the sediment load to adjust from the upstream
 392 disruption to the equilibrium transport rate. Meanwhile, there is barely any bed degradation at the upstream end after 0.2 year,
 393 in correspondence with the fact that the spatial gradient of q_s becomes quite small. In Table 2 we also exhibit the δ values for

394 this idealized run. It is no surprise that both $\delta(z_b)$ and $\delta(q_s)$ are high, as the entrainment form and flux form predict very different
 395 patterns with such an arbitrarily reduced sediment fall velocity.



396 **Figure 5.** 0.2 year results for the case of uniform sediment using the entrainment form of Exner equation: time variation of (a)
 397 bed elevation z_b and water surface (WS), (b) sediment load per unit width q_s of the LYR in response to the cutoff of sediment
 398 supply. Sediment fall velocity v_s is arbitrarily multiplied by a factor of 0.05 while holding bed grain size constant in this run.
 399 The inset shows detailed results near the upstream end.
 400

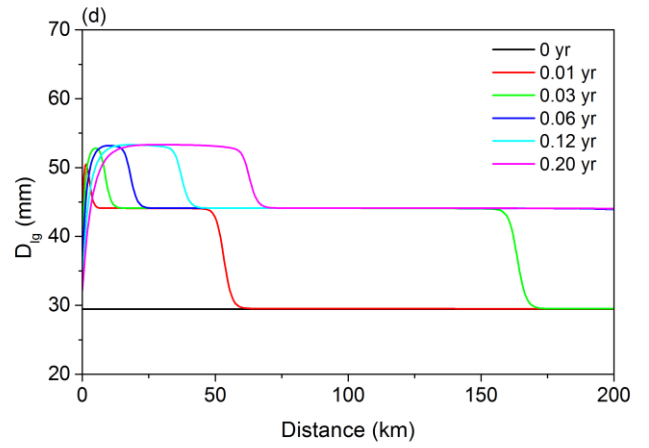
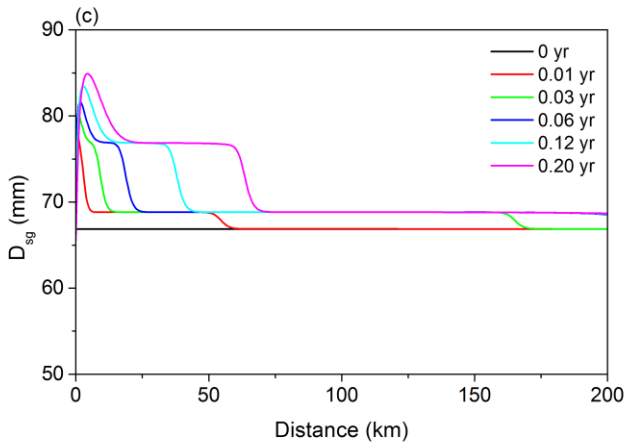
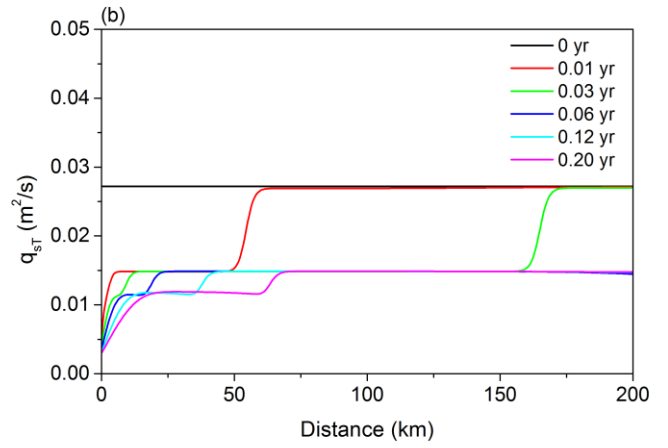
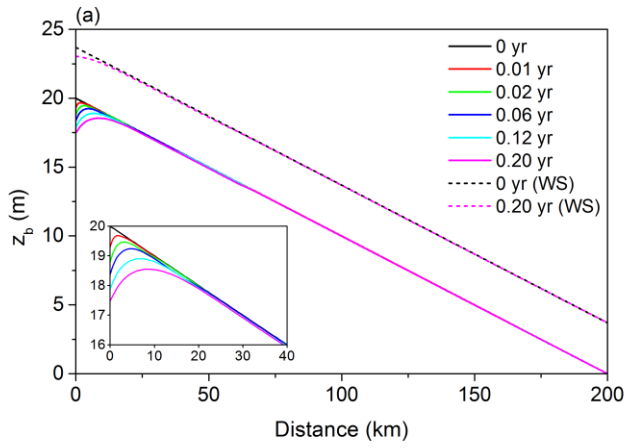
401 ~~In Section 3.1 of the main text, we compare the flux-based morphodynamics and entrainment-based morphodynamics~~
 402 ~~of uniform sediment, under constant water discharge and sediment supply. The aim is to focus on the comparison of the two~~
 403 ~~formulations without being distracted by the complexity of boundary conditions.~~ In Section S2 of the Supplement, we also
 404 conduct numerical simulations with hydrographs. Results indicate that our conclusions based on constant flow discharge also

405 hold when hydrographs are considered: the flux-form and the entrainment form (with the sediment fall velocity not adjusted)
406 of the Exner equation give very similar prediction using a characteristic grain size of 65 μm .

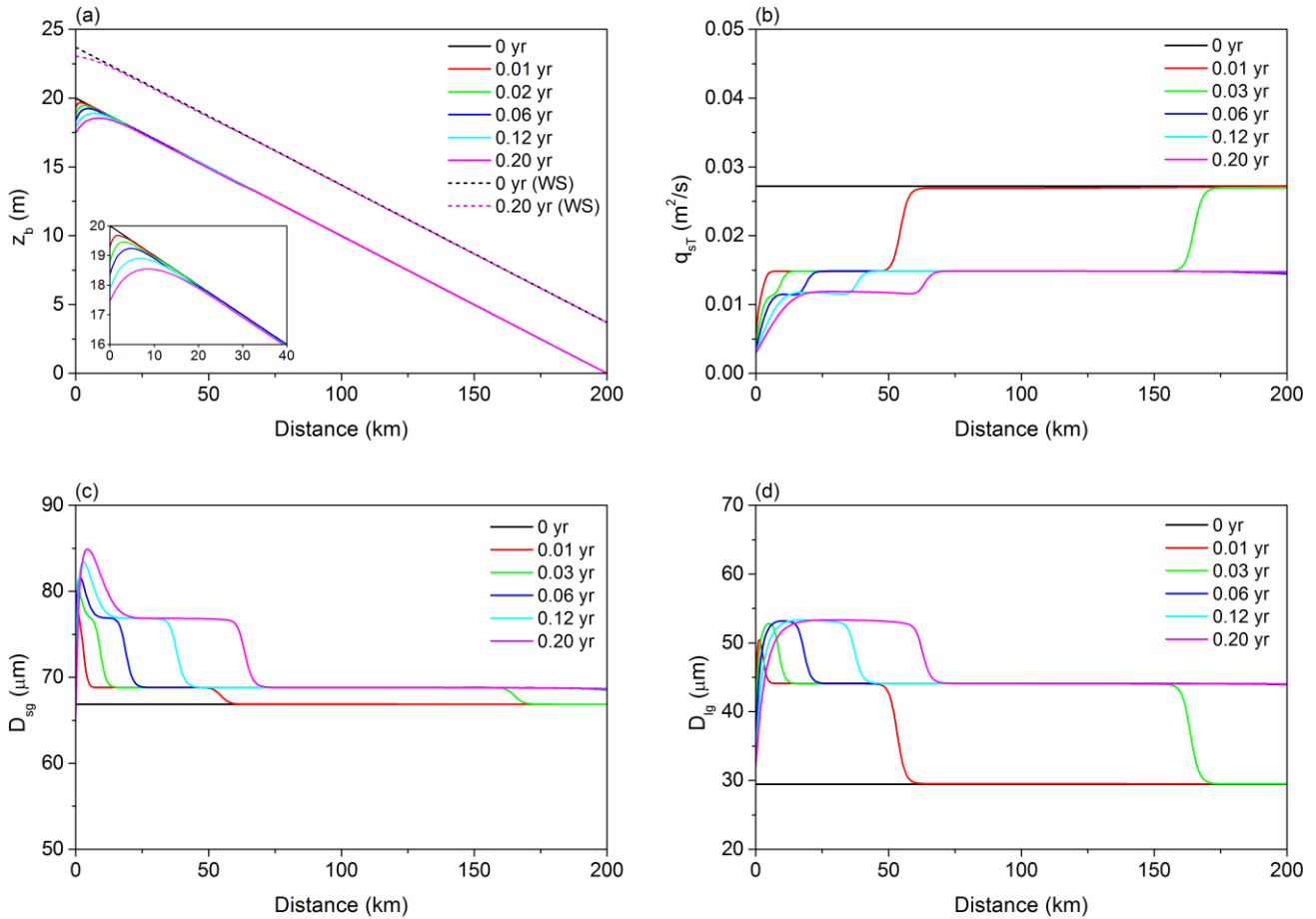
407 3.2 Case of sediment mixtures

408 In this section we consider the morphodynamics of sediment mixtures rather than the case of a uniform bed grain size
409 implemented in section 3.1. The grain size distribution of the initial bed is based on field data at the Lijin gauging station, and
410 is shown in Fig. 2. Using the sediment transport relation of Naito et al. (accepted subject to revision) for mixtures, such a grain
411 size distribution combined with the given bed slope and flow discharge leads to a total equilibrium sediment transport rate per
412 unit width q_{seT} of 0.0272 m^2/s . With a flood intermittency factor I_f of 0.14, this further gives a mean annual bed material load
413 of 95.5 Mt/a. Adding in washload according to the estimate of Naito et al. (accepted subject to revision), total mean annual
414 load 173.7 Mt/a, a value that is of the same order of magnitude as averages over the period 2000-2016 (89-126 Mt/a depending
415 on site), i.e. since the operation of Xiaolangdi Dam in 1999 (Fig. 1(b)). The sediment supply rate of each grain size range is
416 set at 10% of its equilibrium sediment transport rate. This results in a total sediment supply rate of $q_{sf} = 0.00272 \text{ m}^2/\text{s}$, and a
417 grain size distribution of the sediment supply (shown in Fig. 2) that is identical to the grain size distribution of the equilibrium
418 sediment load before the cutoff. That is, the grain size distribution of sediment supply does not change, only the total sediment
419 supply is reduced by 90%. Again we exhibit simulation results for only 0.2 year here, a value that is enough to show the
420 differences between the two forms, flux and entrainment, as applied to mixtures. Modeling results over a longer time scale are
421 presented in Section 4.3.

422 Figure 6 shows the simulation results using the flux form of the Exner equation. As a result of the reduced sediment
423 supply at the inlet, bed degradation occurs first at the upstream end and then gradually migrates downstream. The total sediment
424 transport rate per unit width q_{sT} also reduces as a response to the cutoff of sediment supply. More specifically, the evolution
425 of q_{sT} shows marked evidence of advection, with at least two kinematic waves being observed within 0.2 year. Actually as
426 illustrated by Stecca et al. (2014, 2016), each grain size fraction should induce a migrating wave. As shown in Fig. 6(b), the
427 fastest kinematic wave migrates beyond the 200 km reach within 0.06 year, and the second fastest kinematic wave migrates
428 for a distance of about 60 km in 0.2 year. Figures 6(c) and 6(d) show the results for the surface geometric mean grain size D_{sg}
429 and geometric mean grain size of suspended load D_{lg} respectively. As can be seen therein, both the bed surface and the
430 suspended load coarsen as a result of the cutoff of sediment supply This represents armoring, mediated by the hiding functions
431 of Eqs. (26) and (27). Such coarsening is not evident near the upstream end, possibly due to the inverse slope visible in Fig.
432 6(a). Similarly to the variation of q_{sT} , the patterns of time variation of both D_{sg} and D_{lg} also exhibit very clear kinematic waves,
433 with migration rates about the same as those of q_{sT} .



434



435

436

437

438

439

Figure 6. 0.2 year results for the case of sediment mixtures using the flux form of Exner equation: time variation of (a) bed elevation z_b and water surface (WS), (b) total sediment load q_{sT} , (c) surface geometric mean grain size D_{sg} and (d) geometric mean grain size of sediment load of the LYR in response to the cutoff of sediment supply. The inset shows detailed results near the upstream end.

440

441

442

443

444

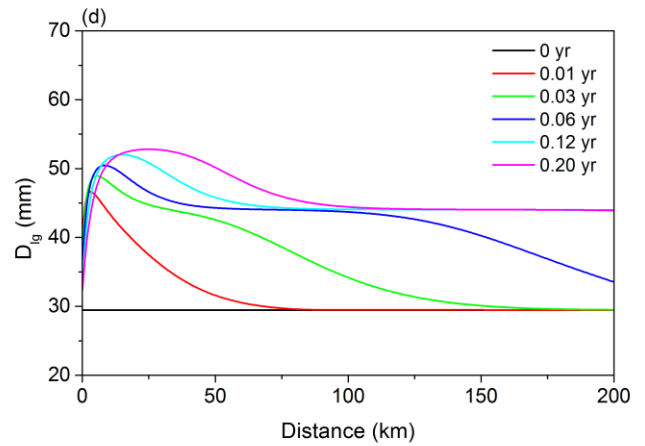
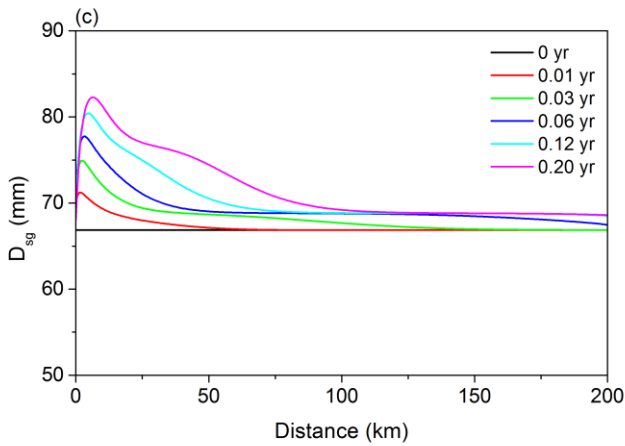
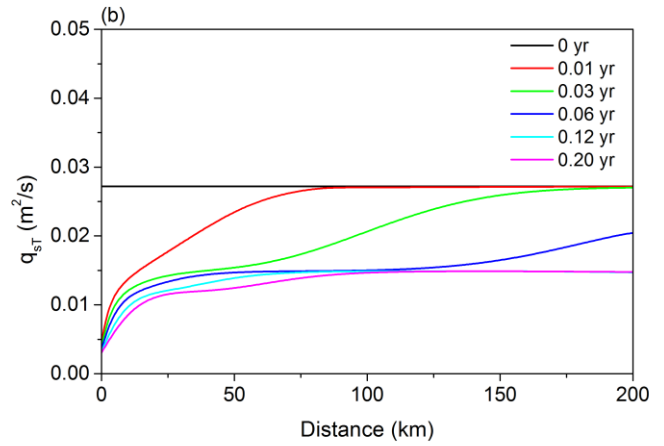
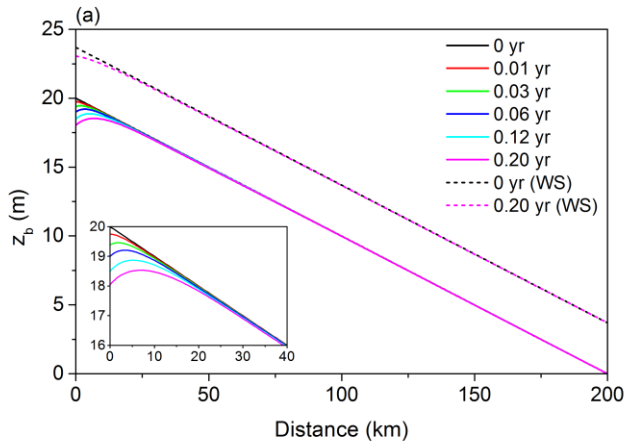
445

446

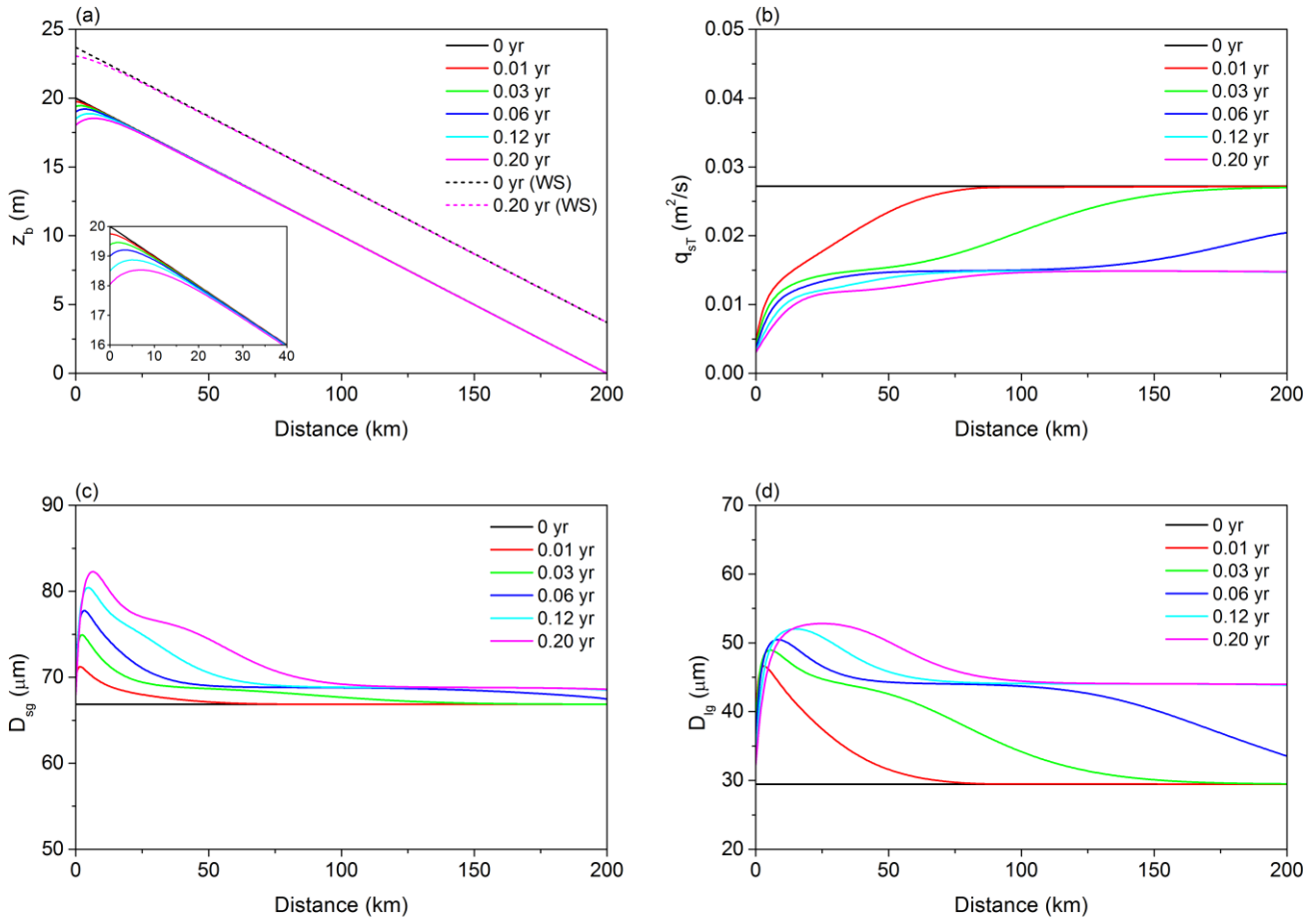
447

Figure 7 shows the simulation results obtained using the entrainment form of the Exner equation. In general, the patterns of variation predicted by the entrainment form have similar trends and magnitudes to those predicted by the flux form: the bed degrades near the upstream end, the suspended load transport rate reduces in time, and both the bed surface and the suspended load coarsen as a result of the cutoff of sediment supply. But the results based on the two forms exhibit very evident differences when multiple grain sizes are included. That is, the results predicted by the entrainment form are sufficiently diffusive so that the variations of q_{sT} , D_{sg} , and D_{lg} (Figs. 7(b), 7(c) and 7(d)) do not show the advective character seen in Fig. 6. Figure 7c, however, shows the same armoring as in the case of calculations with the flux form. No clear kinematic waves can be observed in Fig. 7. Table 3 gives a summary of the values of δ in the case of sediment mixtures. The prediction of bed

448 elevation is not affected much when multiple grain sizes are considered, with $\delta(z_b)$ being no more than 3.5% within 0.2 year.
 449 The δ values of q_{sT} , D_{sg} , and D_{lg} are, however, relatively large since the two forms predict quite different patterns of variations,
 450 as shown in Fig. 6 and Fig. 7.



451



452

453

454

455

456

Figure 7. 0.2 year results for the case of sediment mixtures using the entrainment form of Exner equation: time variation of (a) bed elevation z_b and water surface (WS), (b) total sediment load q_{sT} , (c) surface geometric mean grain size D_{sg} and (d) geometric mean grain size of sediment load of the LYR in response to the cutoff of sediment supply. The inset shows detailed results near the upstream end.

457

458

Table 3. Quantification of the difference between predictions of the flux form and the entrainment form in the case of sediment mixtures. The maximum values of δ in the calculational domain are presented at different times.

		0.01 yr	0.03 yr	0.06 yr	0.12 yr	0.20 yr
original v_s	$\delta(z_b)$	2.3 %	3.2 %	3.4 %	3.4 %	3.2 %
	$\delta(q_{sT})$	54.7 %	76.1 %	41.1 %	10.5 %	11.8 %
	$\delta(D_{sg})$	10.1 %	8.6 %	7.2 %	6.0 %	5.4 %
	$\delta(D_{lg})$	27.1 %	31.9 %	23.7 %	7.2 %	7.7 %
v_s multiplied by 20	$\delta(z_b)$	0.3 %	0.4 %	3.8 %	0.3 %	0.2 %
	$\delta(q_{sT})$	81.1 %	82.3 %	39.7 %	7.2 %	9.3 %
	$\delta(D_{sg})$	2.8 %	2.8 %	2.0 %	2.7 %	3.4 %

459

460

461

462

463

464

465

466

467

468

469

470

471

472

473

474

475

476

477

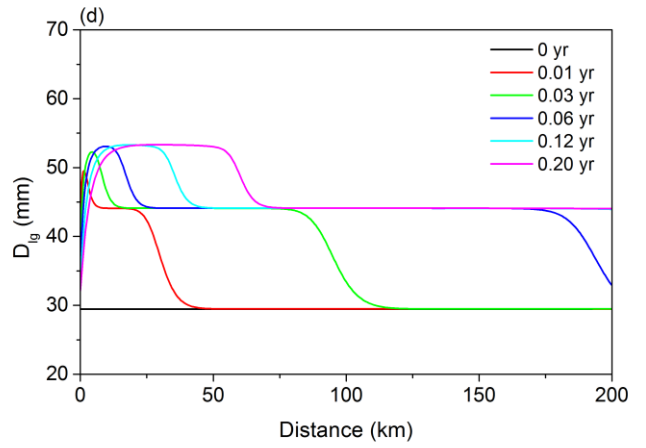
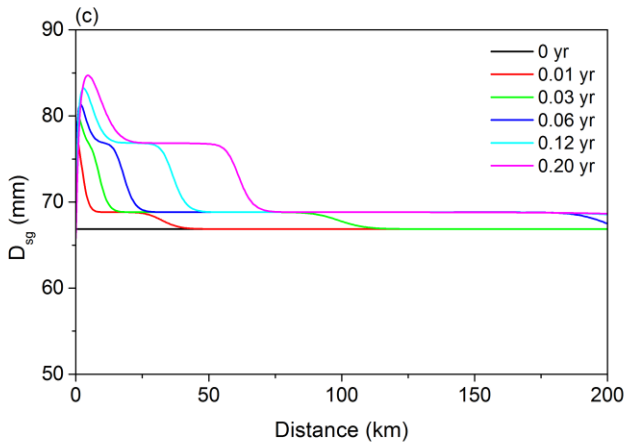
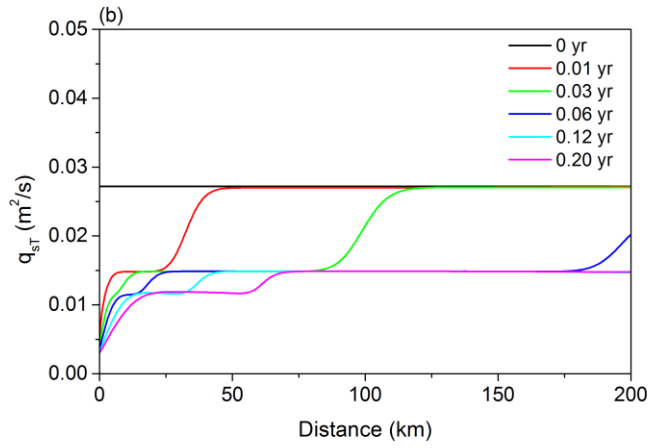
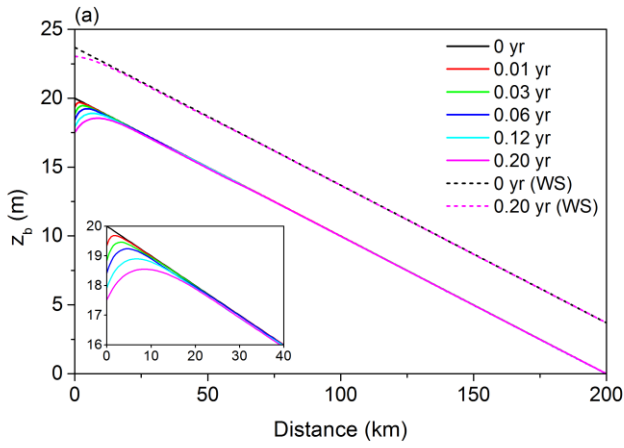
478

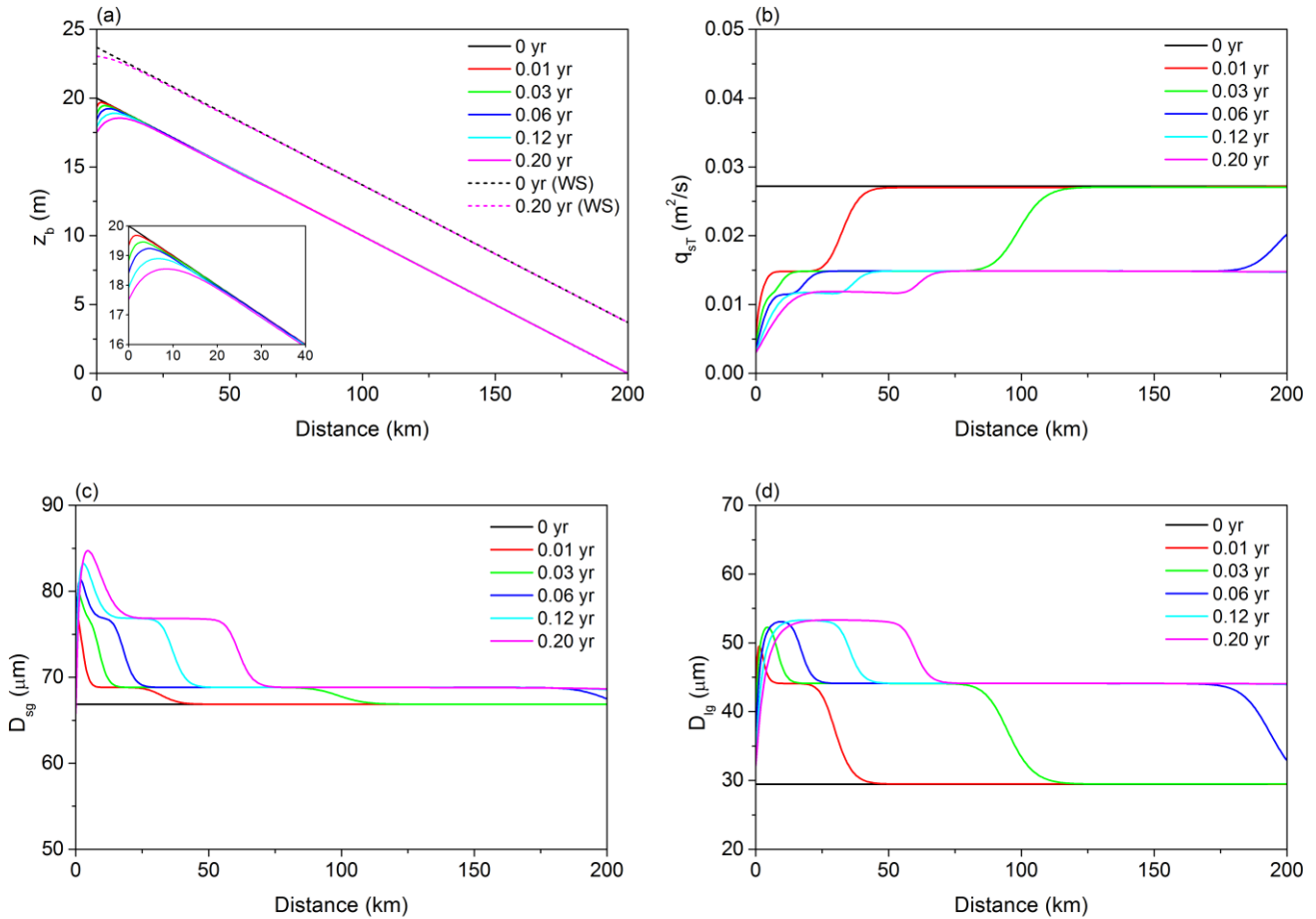
479

480

The results shown in Fig. 8 have also been calculated using the entrainment form of the Exner equation, but here the sediment fall velocities v_{si} used in Eqs. (14)-(16) are arbitrarily multiplied by a factor of 20. That is, we still apply the grain size distribution in Fig. 2, but the sediment fall velocities implemented in the simulation are 20 times the corresponding fall velocities calculated by the relation of Dietrich (1982). In the case of uniform sediment in Section 3.1, we arbitrarily reduce the sediment fall velocity to force a difference between the predictions from the entrainment form and those from the flux form. Here we arbitrarily increase the sediment fall velocity with the aim of determining under what conditions the sorting patterns predicted by the two forms converge. As we can see in Fig. 8, with such a larger and intentionally unrealistic sediment fall velocity, the general trend of variations predicted by the entrainment form does not change, but the results show a notably less diffusive pattern. The variations of q_{sT} , D_{sg} , and D_{lg} show more advection compared with Fig. 7, and at least two kinematic waves appear within 0.2 year. It should be noted that even though these kinematic waves appear after we arbitrarily increase the sediment fall velocity, they are more diffusive than those obtained from the flux formulation and also migrate with a slower celerity as compared with those predicted by the flux form, especially for the fastest kinematic wave in the modeling results.

Table 3 summarizes the δ values for this run. The values of $\delta(z_b)$ become smaller with arbitrarily increased sediment fall velocities except for $t = 0.06$ year. A relatively large value of $\delta(z_b)$ at $t = 0.06$ year occurs near the downstream end of the channel, where the entrainment form predicts some slight degradation. Also, $\delta(q_{sT})$ is quite large at $t = 0.01$ year and 0.03 year, even though the results for the case of increased fall velocities become qualitatively more similar to the prediction of the flux form. This is because the flux form and the entrainment form with arbitrarily increased sediment fall velocities predict different celerities for the fastest kinematic wave. The error $\delta(q_{sT})$ becomes smaller from $t = 0.06$ year as the fastest kinematic wave migrates beyond the channel reach. The error $\delta(D_{lg})$ behaves similarly to $\delta(q_{sT})$, with $\delta(D_{lg})$ being quite large at $t = 0.01$ year and 0.03 year near the fastest kinematic wave, but gradually becoming smaller as time passes. The error $\delta(D_{sg})$ stays low within the whole 0.2-year period, possibly because the fastest kinematic wave of D_{sg} has a small magnitude, as shown in Fig. 8(c).





482

483

484

485

486

487

Figure 8. 0.2 year results for the case of sediment mixtures using the entrainment form of Exner equation: time variation of (a) bed elevation z_b and water surface (WS), (b) total sediment load q_{ST} , (c) surface geometric mean grain size D_{sg} and (d) geometric mean grain size of sediment load of the LYR in response to the cutoff of sediment supply. Sediment fall velocities v_{st} are arbitrarily multiplied by a factor of 20 in this run while keeping the grain sizes invariant. The inset shows detailed results near the upstream end.

488

489

490

491

492

In Section S3 of the Supplement, we conduct additional numerical cases which are similar to the cases in this section, except that hydrographs are implemented instead of constant discharge. Results indicate that our conclusions based on constant flow discharge also hold when hydrographs are considered. The flux form and the entrainment form (with the sediment fall velocity not adjusted) of the Exner equation predict quite different patterns of grain sorting, with the flux form exhibiting more advective character than the entrainment form.

493 4. Discussion

494 4.1 Adjustment of sediment load and the adaptation length

495 In Section 3.1, our simulation shows that in the case of uniform sediment, the flux form and the entrainment form of
496 the Exner equation give very similar predictions for a given sediment size of 65 μm . However, if we arbitrarily reduce the
497 sediment fall velocity by a multiplicative factor of 0.05, the prediction given by the entrainment form will become much more
498 diffusive, in terms of both z_b and q_s . The diffusive nature of the entrainment form as well as the important role played by the
499 sediment fall velocity can be explained in terms of the governing equation.

500 In the entrainment form, the equation governing suspended sediment concentration is,

$$501 \frac{1}{I_f} \frac{\partial(hC)}{\partial t} + \frac{\partial(huC)}{\partial x} = v_s (E - r_0 C) \quad (29)$$

502 i.e. the same as Eq. (4911). The sediment transport rate per unit width $q_s = huC = q_w C$, and the dimensionless entrainment rate
503 $E = r_0 q_{se} / q_w$. In order to simplify the mathematical analysis, here we consider only the adjustment of sediment concentration in
504 space and neglect the temporal derivative in Eq. (29), so that we get

$$505 \frac{\partial q_s}{\partial x} = v_s (E - r_0 C) = \frac{1}{L_{ad}} (q_{se} - q_s) \quad (30)$$

$$506 L_{ad} = \frac{q_w}{v_s r_0} \quad (31)$$

507 where L_{ad} can be identified as the adaptation length for suspended sediment to reach equilibrium. This definition of adaptation
508 length is similar to those in Wu and Wang (2008), and Ganti et al. (2014).

509 If we consider the spatial adjustment of sediment load shortly after the cutoff of sediment supply, we can further
510 neglect the nonuniformity of the capacity (equilibrium) transport rate q_{se} along the channel, and Eq. (30) can be solved with a
511 given upstream boundary condition. That is, with the boundary condition

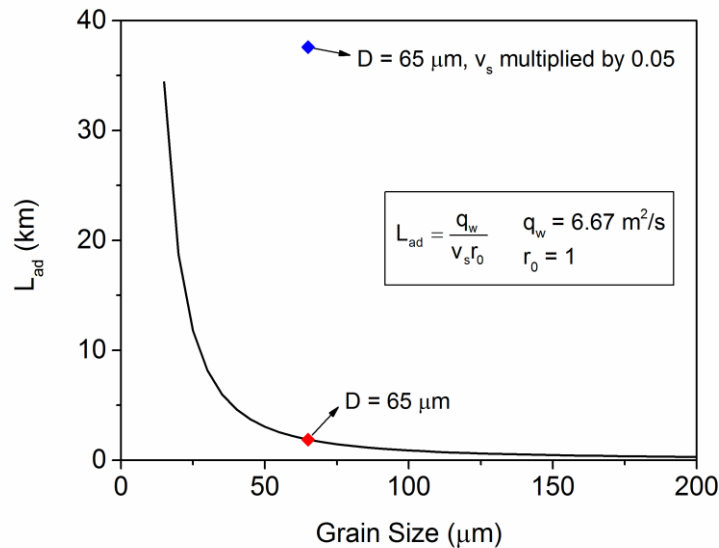
$$512 q_s \Big|_{x=0} = q_{sf} \quad (32)$$

513 Eq. (30) can be solved to yield

$$514 q_s = q_{se} + (q_{sf} - q_{se}) e^{-\frac{x}{L_{ad}}} \quad (33)$$

515 Here q_{sf} is the sediment supply rate per unit width at the upstream end. According to Eq. (33), q_s adjusts exponentially in space
 516 from q_{sf} to q_{se} , which also coincides with our simulation results in Section 3.1, as shown in Figs. 3-6. The adaptation length
 517 L_{ad} is the key parameter that controls the distance for q_s to approach the equilibrium sediment transport rate q_{se} . More
 518 specifically, q_s attains $1 - 1/e$ (i.e. 63.2%) of its adjustment from q_{sf} to q_{se} over a distance L_{ad} . Therefore, the larger the adaptation
 519 length, the slower q_s adjusts in space, so that the more evident lag effects and diffusivity are exhibited in the entrainment form.
 520 In the flux form, however, the sediment load responds simultaneously with the flow conditions, so that $L_{ad} = 0$ and $q_s = q_{se}$
 521 along the entire channel reach.

522 For the case of uniform sediment in Section 3.1, $q_w = 6.67 \text{ m}^2/\text{s}$ and r_0 is specified as unity. Therefore, the value of
 523 L_{ad} is determined only by the sediment fall velocity v_s . Figure 9 shows the value of the adaptation length L_{ad} for various
 524 sediment grain sizes, with the sediment fall velocity v_s calculated by the relation of Dietrich (1982). From the figure we can
 525 see that L_{ad} decreases sharply with the increase of grain size, indicating that the lag effects between sediment transport and
 526 flow conditions are evident for very fine sediment but gradually disappear when sediment is sufficiently coarse. For the
 527 sediment grain size of $65 \mu\text{m}$ implemented in Section 3.1, the corresponding $L_{ad} = 1.88 \text{ km}$, which is much smaller than the
 528 200 km reach of the computational domain. In this case and in general, the predictions of the flux form and the entrainment
 529 form show little difference when $L_{ad}/L \ll 1$, where L is domain length. However, if we arbitrarily multiply the sediment fall
 530 velocity by a factor of 0.05, then L_{ad} becomes 37.60 km . With such a large adaptation length, it is no surprise that the
 531 entrainment form gives very different predictions from the flux form.



532
 533 **Figure 9.** Relation between adaptation length L_{ad} and grain size D . The values of flow discharge per unit width q_w and recovery
 534 coefficient r_0 are the same as those in Section 3.1. The relation of Dietrich (1982) is implemented for sediment fall velocity.

535 The evolution of bed elevation z_b can also be affected by the value of L_{ad} . For example in the case of uniform sediment
 536 in Section 3.1, the flux form corresponds to an adaption length of zero. As a result, the flux form yields a spatial derivative of
 537 q_s near the upstream end that is relatively large, thus leading to fast degradation from the upstream end. In the case of the
 538 entrainment form, however, the spatial derivative of q_s is small with a large L_{ad} , thus leading to a slower and more diffusive
 539 bed degradation. This is especially evident when we arbitrarily reduce the sediment fall velocity by a factor of 0.05, while
 540 keeping grain size invariant.

541 The above analysis also holds for sediment mixtures, except that each grain size range will have its own adaptation
 542 length. Here we neglect the temporal derivative in Eq. (29) and analyze only the spatial adjustment of sediment load. If we
 543 neglect the spatial derivative in Eq. (29) and conduct a similar analysis for sediment concentration, we would find that the
 544 temporal adjustment of sediment concentration is also described by an exponential function of time, in analogy to Eq. (33).

545 **4.2 Patterns of grain sorting: advection vs. diffusion**

546 In Section 3.2 we find that the flux form and entrainment form of the Exner equation provide very different patterns
 547 of grain sorting for sediment mixtures: kinematic sorting waves are evident in the flux form but are diffused out in the
 548 entrainment form. The diffusivity of grain sorting becomes smaller and the kinematic waves appear, however, if we arbitrarily
 549 increase the sediment fall velocity by a factor of 20. In this section, we explain this behavior by analyzing the governing
 550 equations.

551 First we rewrite the sediment transport relation of Naito et al. (accepted subject to revision) in the following form,

$$552 \quad q_{sei} = F_i q_{ri} \quad (34)$$

$$553 \quad q_{ri} = \frac{u_*^3}{RgC_f} A_i \left(\tau_g^* \frac{D_g}{D_i} \right)^{B_i} \quad (35)$$

554 Substituting Eq. (34) into Eq. (6), which is the governing equation for surface fraction F_i in the flux form, we get

$$555 \quad \frac{1}{I_f} (1 - \lambda_p) \left[L_a \frac{\partial F_i}{\partial t} + (F_i - f_{li}) \frac{\partial L_a}{\partial t} \right] = f_{li} \frac{\partial \sum_{j=1}^n F_j q_{rj}}{\partial x} - \frac{\partial F_i q_{ri}}{\partial x} \quad (36)$$

556 Equation (36) can be written in the form of a kinematic wave equation with source terms as below,

$$557 \quad \frac{\partial F_i}{\partial t} + c_{Fi} \frac{\partial F_i}{\partial x} = SF_i \quad (37)$$

$$558 \quad c_{Fi} = \frac{I_f q_{ri}}{(1-\lambda_p)L_a} (1-f_{li}) \quad (38)$$

$$559 \quad SF_i = -\frac{I_f F_i (1-f_{li})}{(1-\lambda_p)L_a} \frac{\partial q_{ri}}{\partial x} + \frac{I_f f_{li}}{(1-\lambda_p)L_a} \frac{\partial \sum_{j=1}^{n, j \neq i} F_j q_{rj}}{\partial x} - \frac{F_i - f_{li}}{1-\lambda_p} \frac{\partial L_a}{\partial t} \quad (39)$$

560 where c_{Fi} is the i -th celerity of kinematic wave and SF_i denotes source terms. Since the surface geometric mean grain size D_{sg} ,
561 the total sediment load per unit width q_{sT} (which equals the equilibrium sediment transport rate q_{seT}), and the geometric mean
562 grain size of sediment load D_{lg} are all closely related to the surface grain size fractions F_i , the evolution of these three
563 parameters shows marked advective behavior when simulated by the flux form of the Exner equation. However, the evolution
564 of bed elevation z_b is related to $\partial q_{sT}/\partial x$, which is dominated by diffusion if q_{sT} is predominantly slope-dependent (as is the
565 case here). The advection-diffusion character of the flux form of Exner equation for sediment mixtures has been documented
566 thoroughly in a series of papers (e.g. Stecca et al., 2014; Stecca et al., 2016; An et al., 2017). The reader can reference these
567 papers for more details.

568 Now we turn to the entrainment form of the Exner equation. Combined with the sediment transport rate per unit width
569 $q_{si} = huC_i = q_w C_i$ and the dimensionless entrainment rate $E_{i-} = r_{0i} q_{sei}/q_w$, Eq. (16) and Eq. (15) can be written as,

$$570 \quad \frac{1}{I_f} \frac{\partial \left(\frac{q_{si}}{u} \right)}{\partial t} + \frac{\partial q_{si}}{\partial x} = \frac{v_{si} r_{0i}}{q_w} (q_{sei} - q_{si}) \quad (40)$$

$$571 \quad \frac{1}{I_f} (1-\lambda_p) \left[L_a \frac{\partial F_i}{\partial t} + (F_i - f_{li}) \frac{\partial L_a}{\partial t} \right] = f_{li} \sum_{j=1}^n \frac{v_{sj} r_{0j}}{q_w} (q_{sej} - q_{sj}) - \frac{v_{si} r_{0i}}{q_w} (q_{sei} - q_{si}) \quad (41)$$

572 where Eq. (40) denotes the conservation of suspended sediment and Eq. (41) denotes the conservation of bed material. If we
573 rewrite Eq. (40) in the following form,

$$574 \quad q_{si} = q_{sei} - \frac{q_w}{v_{si} r_{0i}} \left[\frac{1}{I_f} \frac{\partial \left(\frac{q_{si}}{u} \right)}{\partial t} + \frac{\partial q_{si}}{\partial x} \right] \quad (42)$$

575 then q_{si} can be solved iteratively. With an initial guess of $q_{si} = q_{sei}$ and neglecting the temporal derivatives, we obtain the second
576 order solution of q_{si} as,

$$577 \quad q_{si} = q_{sei} - \frac{q_w}{v_{si}r_{oi}} \frac{\partial}{\partial x} \left(q_{sei} - \frac{q_w}{v_{si}r_{oi}} \frac{\partial q_{sei}}{\partial x} \right) \quad (43)$$

578 Details of the iteration scheme are given in Section S4 of the Supplement.

579 Substituting Eq. (43) and Eq. (34) into Eq. (41), we find that

$$580 \quad \frac{1}{I_f} (1 - \lambda_p) \left[L_a \frac{\partial F_i}{\partial t} + (F_i - f_{li}) \frac{\partial L_a}{\partial t} \right] = f_{li} \sum_{j=1}^n \frac{\partial}{\partial x} \left(F_j q_{rj} - \frac{q_w}{v_{sj}r_{oj}} \frac{\partial F_j q_{rj}}{\partial x} \right) - \frac{\partial}{\partial x} \left(F_i q_{ri} - \frac{q_w}{v_{si}r_{oi}} \frac{\partial F_i q_{ri}}{\partial x} \right) \quad (44)$$

581 Expanding out the last two terms in Eq. (44) using the chain rule, after some work the relation for the conservation of bed
582 material can be expressed as,

$$583 \quad \frac{\partial F_i}{\partial t} + c_{Ei} \frac{\partial F_i}{\partial x} - v_i \frac{\partial^2 F_i}{\partial x^2} = SE_i \quad (45)$$

$$584 \quad c_{Ei} = \frac{(1 - f_{li}) I_f}{(1 - \lambda_p) L_a} \left(q_{ri} - 2 \frac{q_w}{v_{si}r_{oi}} \frac{\partial q_{ri}}{\partial x} \right) \quad (46)$$

$$585 \quad v_i = \frac{(1 - f_{li}) I_f q_w q_{ri}}{(1 - \lambda_p) L_a v_{si} r_{oi}} \quad (47)$$

$$586 \quad SE_i = \frac{I_f f_{li}}{(1 - \lambda_p) L_a} \sum_{j=1}^{n, j \neq i} \frac{\partial}{\partial x} \left(F_j q_{rj} - \frac{q_w}{v_{sj}r_{oj}} \frac{\partial F_j q_{rj}}{\partial x} \right) - \frac{(1 - f_{li}) I_f}{(1 - \lambda_p) L_a} \left(F_i \frac{\partial q_{ri}}{\partial x} - \frac{q_w}{v_{si}r_{oi}} F_i \frac{\partial^2 q_{ri}}{\partial x^2} \right) - \frac{F_i - f_{li}}{L_a} \frac{\partial L_a}{\partial t} \quad (48)$$

587 where c_{Ei} is the celerity of kinematic wave, v_i is the diffusivity coefficient, and SE_i denote source terms.

588 From Eq. (45) we can see that the governing equation for F_i in the entrainment form is an advection-diffusion equation,
589 rather than the kinematic wave equation of the flux form. The surface geometric mean grain size D_{sg} is governed by Eq. (45),
590 with describes the variation of the surface fractions F_i from which it is computed. The equilibrium sediment transport rate q_{sei}
591 is governed by Eq. (45) because we implement a surface-based sediment transport relation as shown in Eq. (34). According to
592 Eq. (43), the total sediment load per unit width q_{st} and the geometric mean grain size of sediment load D_{lg} must also be closely
593 related to the surface grain size fractions F_i . Therefore, the diffusion terms in Eq. (45) can lead to dissipation of the kinematic
594 waves in Figs. 7(b), 7(c), and 7(d).

595 From Eq. (47), we can also see that the diffusivity coefficient v_i is related to the sediment fall velocity v_{si} : the larger
 596 the sediment fall velocity, the smaller the diffusivity coefficient. Thus when we increase the sediment fall velocity arbitrarily
 597 by a factor of 20 in Section 3.2, the kinematic waves become more evident as a result of the reduction of diffusivity.

598 Moreover if we compare the celerity of kinematic waves in both the flux form and the entrainment form, we have

$$599 \frac{c_{Ei}}{c_{Fi}} = 1 - r_{ci} \quad (49)$$

$$600 r_{ci} = 2 \frac{L_{adi}}{q_{ri}} \frac{\partial q_{ri}}{\partial x} \quad (50)$$

601 where L_{adi} is the adaptation length for the i -th size range as defined by Eq. (31). More specifically, the value of r_{ci} depends on
 602 $\partial q_{ri} / \partial x$. For our numerical simulation in Section 3.2, $\partial q_{ri} / \partial x > 0$ as a result of bed degradation progressing from the upstream
 603 end, thus leading to a positive value of r_{ci} and an entrainment celerity c_{Ei} that is smaller than the corresponding flux celerity
 604 c_{Fi} . This is consistent with our numerical results: the kinematic waves in Fig. 8 predicted by the entrainment form are somewhat
 605 smaller than the kinematic waves in Fig. 6 predicted by the flux form.

606 4.3 Modeling implications and limitations

607 In Section 3, two numerical cases are conducted to compare the flux form and the entrainment form of the Exner
 608 equation, but only within 0.2 year after the cutoff of sediment supply. Here we run both numerical cases for a longer time (5
 609 years). Table 4 shows the results of the case of uniform sediment (as described in Section 3.1) within 5 years, and Table 5
 610 shows the results of the case of sediment mixtures (as described in Section 3.2) within 5 years. For both cases, the δ values,
 611 corresponding to relative deviation between the flux and entrainment forms, become quite small after 1 year, thus validating
 612 our assumption that the predictions of the two forms tend to be most evident shortly after disruption, but gradually diminish
 613 over a longer time scale. Moreover, if the water and sediment supply are kept constant for a sufficiently long time, the flux
 614 form and entrainment form of Exner equation predict exactly the same equilibrium, in terms of both the channel slope and the
 615 bed surface texture. Under such conditions, the sediment transport rate (of each size range) equals to the equilibrium sediment
 616 transport rate (of each size range), and also equals to the sediment supply rate (of each size range).

617 **Table 4.** Quantification of the difference between predictions of the flux form and the entrainment form in the case of uniform
 618 sediment. The maximum δ in the calculational domain are presented for each of 5 years.

		1 yr	2 yr	3 yr	4 yr	5 yr
original v_s	$\delta(z_b)$	3.0 %	2.7 %	2.6 %	2.5 %	2.6 %
	$\delta(q_s)$	3.0 %	1.8 %	1.3 %	1.1 %	1.0 %

619

620 **Table 5.** Quantification of the difference between predictions of the flux form and the entrainment form in the case of sediment
 621 mixtures. The maximum δ in the calculational domain are presented for each of five years.

		1 yr	2 yr	3 yr	4 yr	5 yr
original v_s	$\delta(z_b)$	2.2 %	1.9 %	1.7 %	1.7 %	1.7 %
	$\delta(q_{sT})$	2.9 %	1.8 %	1.5 %	1.4 %	3.9 %
	$\delta(D_{sg})$	5.2 %	3.9 %	3.5 %	4.7 %	3.9 %
	$\delta(D_{lg})$	0.7 %	0.6 %	1.0 %	1.3 %	0.8 %

622

623

624

625

626

627

628

629

630

631

632

633

634

635

636

637

638

639

640

641

642

643

644

645

646

647

Based on the numerical modeling and mathematical analysis in this paper, we suggest that the entrainment form of the Exner equation be used when studying the river morphodynamics of fine-grained sediment (or more specifically sediment with small fall velocity). This is because the adaptation length L_a and the diffusivity coefficient v_i are large for fine sediment, but the flux form of the Exner equation does not account for lag effects or diffusivity of individual size fractions, thus leading to unrealistic simulation results. Such unrealistic simulation results can include an overestimation of advection as sediment sorts (as shown in the case of sediment mixtures) and an overestimation of the aggradation/degradation rate (as shown in the case of uniform sediment) when sufficiently small grain sizes (or sediment fall velocities) are considered. [Field survey of the LYR observes no clear sorting waves: the grain size distribution adjusts smoothly both in space and in time, thus indicating that the more physically-based Entrainment form is more applicable in terms of the sorting processes of the LYR.](#) It should be noted, however, that the difference in the predictions of the two forms of Exner equation tends to be large shortly after disruption, but gradually diminishes over time. The flux form of the Exner equation, on the other hand, is particularly applicable for coarse sediment, or when the sediment transport is dominated by bedload (e.g. gravel-bed rivers). The above results could have practical implications in regard to a wide range of issues including dam construction, water and sediment regulation, flood management, and ecological restoration schemes. The results can also be used as a reference for other fine-grained fluvial systems similar to the LYR, such as the Pilcomayo River in Paraguay/Argentina, South America (Martín-Vide et al., 2014).

It should be noted that in the morphodynamic models of this paper, we implement the mass and momentum conservation equations for clear water (i.e., Eq. (1) and Eq. (2)) to calculate flow hydraulics, instead of the mass and momentum equations for water-sediment mixture as suggested by Cao et al. (2004) and Cao et al. (2006). More specifically, Cui et al. (2005) have pointed out that when sediment concentration in the water is sufficiently small, bed elevation can be taken to be unchanging over characteristic hydraulic time scales, and the effects of flow-bed exchange on flow hydraulics can be neglected. For the two simulation cases in this paper, the volume sediment concentration C drops from about 2×10^{-3} to about 2×10^{-4} in the case of uniform sediment, and from about 4×10^{-3} to about 4×10^{-4} in the case of sediment mixtures, due to the cutoff of sediment supply at the upstream end. These dilute concentrations validate our implementation of mass and momentum conservation equations for clear water. Our assumption is not necessarily correct for the entire Yellow River. Upstream of our study reach, and especially upstream of Sanmenxia Dam, the flow is often hyperconcentrated (Xu, 1999).

648 Considering the fact that in our numerical simulations a constant inflow discharge (along with a flood intermittency
649 factor) is implemented, and also considering that the morphodynamic time scale is much larger than the hydraulic time scale
650 in our case, the quasi-steady approximation or even the normal flow approximation can be introduced to further save
651 computational efforts (Parker, 2004). But one thing that should be noted is that in our simulation results in Section 3, the bed
652 exhibits an inverse slope near the upstream end. The normal flow assumption becomes invalid under such circumstances, so
653 requiring a full unsteady shallow water model.

654 By definition, the recovery coefficient r_o is the ratio of the near-bed to the flux-depth-averaged concentration of
655 suspended load, and is thus related to the concentration profile. In our simulation r_o is specified as unity. That is, density
656 stratification effects of suspended sediment are neglected, and the vertical profile of sediment concentration is regarded as
657 uniform. However in natural rivers, the value of r_o can vary significantly under different circumstances (Cao et al., 2004; Duan
658 and Nanda, 2006; Zhang and Duan, 2011; Zhang et al., 2013). In general, the value of r_o is no less than unity and can be as
659 large as 12 (Zhang and Duan, 2011). Therefore according to our mathematical analysis in Section 4.1 and 4.2, $r_o = 1$
660 corresponds to a maximum adaptation length L_{ad} , a maximum diffusivity coefficient ν_i , and a minimum ratio of celerities c_{Ei}/c_{Fi} ,
661 thus leading to the largest difference between the flux form and the entrainment form. When sediment concentration is
662 sufficiently high, hindered settling effects reduce the sediment fall velocity. Considering the fact that the sediment
663 concentrations considered in our simulation are fairly small, hindered settling effects are not likely significant. More study on
664 stratification and hindered settling effects would be useful in the case of the LYR.

665 In this paper, a one-dimensional morphodynamic model with several simplifications is implemented to compare the
666 flux-based Exner equation and the entrainment-based Exner equation in context of the LYR. However, a site-specific model
667 of the morphodynamics of the LYR without these simplifications would be much more complex. For example, in our 1D
668 simulation we observe bed degradation after the closure of the Xiaolangdi Dam, but we cannot resolve its structure in the
669 lateral direction. In natural rivers, bed degradation is generally not uniform across the channel width, but may be concentrated
670 in the thalweg. Moreover, the spatial variation of channel width and initial slope, which are not considered in this paper, are
671 also important when considering applied problems. The above-mentioned issues, even though not the aim of this paper, merit
672 future research (e.g. He et al., 2012). Besides, Chavarrias et al. (2018) have reported that morphodynamic models considering
673 mixed grain sizes may be subject to ~~numerical~~ instabilities that result from complex eigenvalues of the system of equations
674 not easily remedied. No such instabilities were encountered in the present work.

675 5 Conclusion

676 In this paper, we compare two formulations for sediment mass conservation in context of the Lower Yellow River,
677 i.e. the flux form of the Exner equation and the entrainment form of the Exner equation. We represent the flux form in terms
678 of as based on the local capacity sediment transport rate, and the entrainment form in terms of as based on the local capacity
679 entrainment rate. In the flux form of the Exner equation, the conservation of bed material is related to the streamwise gradient

680 of sediment transport rate, which is in turn computed based on the quasi-equilibrium assumption according to which the local
681 sediment transport rate equals the capacity rate. In the entrainment form of the Exner equation, on the other hand, the
682 conservation of bed material is related to the difference between the entrainment rate of sediment from the bed into the flow
683 and the deposition rate of sediment from the flow onto the bed. A nonequilibrium sediment transport formulation is applied
684 here, so that the sediment transport rate can lag in space and time behind changing flow conditions. Despite the fact that the
685 entrainment form is usually recommended for the morphodynamic modeling of the LYR due to its fine-grained sediment, there
686 has been little discussion of the differences in predictions between the two forms.

687 Here we implement a 1-D morphodynamic model for this problem. The fully unsteady Saint Venant Equations are
688 implemented for the hydraulic calculation. Both the flux form and the entrainment form of Exner equation are implemented
689 for sediment conservation. For each formulation, we include the options of both uniform sediment and sediment mixtures.
690 Two generalized versions of the Engelund-Hansen relation specifically designed for the LYR are implemented to calculate the
691 quasi-equilibrium sediment transport rate (i.e., sediment transport capacity). They are the version of Ma et al. (2017) for
692 uniform sediment, and the version of Naito et al. (accepted subject to revision) for sediment mixtures. The method of Viparelli
693 et al. (2010) is implemented to store and access bed stratigraphy as the bed aggrades and degrades. We apply the
694 morphodynamic model to two cases with conditions typical of the LYR.

695 In the first case, a uniform bed material grain size of 65 μm is implemented. We study the effect of cutoff of sediment
696 supply, as occurred after the operation of Xiaolangdi Dam in 1999. We find that the flux form and the entrainment form give
697 very similar predictions for this case. Through quantification of the difference between the two forms with a normalized
698 measure of relative difference, we find that difference in the prediction of bed elevation is quite small ($< 4\%$), but difference
699 in the prediction of sediment load can be relatively large (about 20%) shortly after the cutoff of sediment supply.

700 The results for the case of uniform sediment can be explained by analyzing the governing equation of sediment load
701 q_s . In the flux form, the volume sediment transport rate per unit width q_s equals to the local equilibrium (capacity) value q_{se} .
702 In the entrainment form, however, we find that the difference between q_s and q_{se} decays exponentially in space. The adaptation
703 length $L_{ad} = q_w / (v_s r_0)$ is the key parameter that controls the distance for q_s to approach its equilibrium value q_{se} . The larger
704 the adaptation length, the more different the predictions of the two forms will be. For computational conditions in this case,
705 the adaption length is relatively small ($L_{ad} = 1.88 \text{ km}$).

706 In the second case the bed material consists of mixtures ranging from 15 μm to 500 μm . We find that the flux form
707 and the entrainment form give very different patterns of grain sorting. Evident kinematic waves occur at various timescales in
708 the flux form, but no evident kinematic waves can be observed in the entrainment form. The different sorting patterns are
709 reflected in the evolution of surface geometric mean grain size D_{sg} , total sediment load q_{sT} and geometric mean grain size of
710 sediment load D_{lg} , but are not reflected in the evolution of bed elevation z_b .

711 The different sorting patterns exhibited in the case of sediment mixtures can be explained by analyzing the governing
712 equation for bed surface fractions F_i , i.e. the grain size-specific conservation of bed material. We find that in the flux form, the
713 governing equation for F_i can be written in the form of a kinematic wave equation. In the entrainment form, however, the

714 governing equation for F_i is an advection-diffusion equation. It is the diffusion term which leads to the dissipation of kinematic
715 waves. Moreover, in the advection-diffusion equation arising from the entrainment form, the coefficient of diffusivity is
716 inversely proportional to the sediment fall velocity. In addition, under the condition of bed degradation the wave celerity is
717 smaller than that arising from the flux form.

718 Overall, our results indicate that the more complex entrainment form of the Exner equation might be required when
719 the sorting processes of fine-grained sediment (or sediment with small fall velocity) is studied, especially at relatively short
720 timescale. Under such circumstances, the flux form of the Exner equation might overestimate advection in sorting processes
721 as well as the aggradation/degradation rate, due to the fact that it cannot account for the relatively large adaptation length or
722 diffusivity of fine particles.

723 **Notation**

724 C depth-flux-averaged sediment concentration

725 C_f dimensionless bed resistance coefficient

726 C_c dimensionless Chezy resistance coefficient

727 c_b near-bed sediment concentration

728 c_E celerity of the kinematic wave corresponding to F_i in the entrainment form

729 c_{F_i} celerity of the kinematic wave corresponding to F_i in the flux form

730 D sediment grain size

731 E dimensionless entrainment rate of sediment

732 F_i volumetric fraction of surface material in the i -th size range

733 f_{fi} volumetric fraction of sediment in the i -th size range exchanged across the surface-substrate interface

734 g gravitational acceleration

735 h water depth

736 I_f flood intermittency factor

737 L_a thickness of active layer

738 L_{ad} adaptation length of suspended load

739 p_{si} volumetric fraction of bed material load in the i -th size range

740 q_{ri} normalized sediment transport rate per unit width for the i -th size range, defined by Eq. (34)

741 q_s volumetric sediment transport rate per unit width

742 q_{se} equilibrium volumetric sediment transport rate (capacity) per unit width

743 q_{sf} sediment supply rate per unit width

744 q_w flow discharge per unit width

745 R submerged specific gravity of sediment

746 r_0 user-specified parameter denoting the ratio between the near-bed sediment concentration and the flux-averaged sediment
747 concentration
748 S bed slope
749 t time
750 u depth-averaged flow velocity
751 u_* shear velocity
752 v_s sediment fall velocity
753 x streamwise coordinate
754 z_b bed elevation
755 α coefficient in Eq. (6) for interfacial exchange fractions
756 Δt_h time step for hydraulic calculation
757 Δt_m time step for morphologic calculation
758 Δx spatial step length.
759 δ normalized parameter quantifying the fraction difference between the entrainment form and the flux form.
760 λ_p porosity of bed deposit
761 ν_i diffusivity coefficient corresponding to F_i in the entrainment form;
762 ρ density of water
763 ρ_s density of sediment
764 τ_b bed shear stress
765 τ^* dimensionless shear stress (Shields number)

766 **Competing interests**

767 The authors declare that they have no conflict of interest.

768 **Acknowledgments**

769 The participation of Chenge An and Xudong Fu was made possible in part by grants from the National Natural Science
770 Foundation of China (grants 51525901 and 91747207), and the Ministry of Science and Technology of China (grant
771 2016YFC0402406). The participation of Andrew J. Moodie, Hongbo Ma, Kensuke Naito, and Gary Parker were made possible
772 in part by grants from National Science Foundation (grant EAR-1427262). The participation of Yuanfeng Zhang was made
773 possible in part by grant from the National Natural Science Foundation of China (grant 51379087). Part of this research was
774 accomplished during Chenge An's visit in the University of Illinois at Urbana-Champaign, which was supported by the China
775 Scholarship Council (file no. 201506210320). The participation of Andrew J. Moodie was also supported by a National Science

776 Foundation Graduate Research Fellowship (grant 145068). We thank the Morphodynamics Class of 2016 at the University of
777 Illinois at Urbana-Champaign for their participation in preliminary modeling efforts. We thank Astrid Blom and two other
778 anonymous reviewers for their constructive comments and remarks, which helped us greatly improve the manuscript.

779 **References**

- 780 An, C., Fu, X., Wang, G., and Parker, G.: Effect of grain sorting on gravel bed river evolution subject to cycled hydrographs:
781 Bed load sheets and breakdown of the hydrograph boundary layer, *Journal of Geophysical Research-Earth Surface*,
782 122, 1513-1533, doi:10.1002/2016JF003994.
- 783 Armanini, A. and Di Silvio, G.: A one-dimensional model for the transport of a sediment mixture in non-equilibrium conditions,
784 *Journal of Hydraulic Research*, 26(3), 275-292, doi:10.1080/00221688809499212, 1988.
- 785 Bell, R. G. and Sutherland, A. J.: Nonequilibrium bedload transport by steady flows, *Journal of Hydraulic Engineering*, 109(3),
786 351-367, 1983.
- 787 Blom, A.: Different approaches to handling vertical and streamwise sorting in modeling river morphodynamics, *Water*
788 *Resources Research*, 44(3), W03415, doi:10.1029/2006WR005474, 2008.
- 789 Blom, A., Viparelli, E., Chavarrás, V.: The graded alluvial river: profile concavity and downstream fining, *Geophysical*
790 *Research Letters*, 43, 1–9, doi:10.1002/2016GL068898, 2016.
- 791 Blom, A., Arkesteijn, L., Chavarrás, V., Viparelli, E.: The equilibrium alluvial river under variable flow and its channel-
792 forming discharge, *Journal of Geophysical Research-Earth Surface*, 122, 1924-1948, doi: 10.1002/2017JF004213,
793 2017.
- 794 Bohorquez, P. and Ancy, C.: Particle diffusion in non-equilibrium bedload transport simulations, *Applied Mathematical*
795 *Modeling*, 40(17-18), 7474-7492, doi:10.1016/j.apm.2016.03.044, 2016.
- 796 Bradley, B. R. and Venditti J G.: Reevaluating dune scaling relations, *Earth-Science Reviews*, 165, 356-376, 2017.
- 797 Brownlie, W. R.: Prediction of flow depth and sediment discharge in open channels, W. M. Keck Laboratory of Hydraulics
798 and Water Resources, California Institute of Technology, Pasadena, USA, Rep. KH-R-43A, 232 pp., 1981.
- 799 Cao, Z., Pender, G., Wallis, S., and Carling, P.: Computational dam-break hydraulics over erodible sediment bed, *Journal of*
800 *Hydraulic Engineering*, 130(7), 689-703, 2004.
- 801 Cao, Z., Pender, G., and Carling, P.: Shallow water hydrodynamic models for hyperconcentrated sediment-laden floods over
802 erodible bed, *Advances in Water Resources*, 29(4), 546-557, doi:10.1016/j.advwatres.2005.06.011, 2006.
- 803 Chavarrás, V., Stecca, G., and Blom, A.: Ill-posedness in modeling mixed sediment river morphodynamics, *Advances in*
804 *Water Resources*, 114, 219-235, doi:10.1016/j.advwatres.2018.02.011, 2018.
- 805 Cui, Y., Parker, G., Lisle T. E., Pizzuto, J. E., and Dodd, A. M.: More on the evolution of bed material waves in alluvial rivers,
806 *Earth Surface Processes and Landforms*, 30, 107-114, doi:10.1002/esp.1156, 2005.

807 Dietrich, E. W.: Settling velocity of natural particles, *Water Resources Research*, 18(6), 1626-1982,
808 doi:10.1029/WR018i006p01615, 1982.

809 Dorrell, R. M. and Hogg, A. J.: Length and time scales of response of sediment suspensions to changing flow conditions,
810 *Journal of Hydraulic Engineering*, 138(5), 430-439, doi:10.1061/(ASCE)HY.1943-7900.0000532, 2012.

811 Duan, J. G. and Nanda, S. K.: Two-dimensional depth-averaged model simulation of suspended sediment concentration
812 distribution in a groyne field, *Journal of Hydrology*, 324(3-4), 426-437, 2006.

813 Einstein, H. A.: Bedload transport as a probability problem, PhD thesis, Mitt. Versuchsanst. Wasserbau Eidg. Tech. Hochsch,
814 Zurich, Switzerland, 1937.

815 El kadi Abderrezzak, K. and Paquier, A.: One-dimensional numerical modeling of sediment transport and bed deformation in
816 open channels, *Water Resources Research*, 45, W05404, doi:10.1029/2008WR007134, 2009.

817 Englund, F. and Hansen, E.: A monograph on sediment transport in alluvial streams, Technisk Vorlag, Copenhagen, Denmark,
818 1967.

819 Exner, F. M.: Uber die Wechselwirkung zwischen Wasser und Geschiebe in Flussen, Sitzber. Akad. Wiss Wien, 134(2a), 169-
820 204, 1920, (in German).

821 Ferguson, R. I. and Church, M.: A simple universal equation for grain settling velocity, *Journal of Sedimentary Research*,
822 74(6), 933-937, doi:10.1306/051204740933, 2004.

823 Ganti, V., Lamb, M. P., and McElroy, B.: Quantitative bounds on morphodynamics and implications for reading the
824 sedimentary record, *Nature Communications*, 5, 3298, doi:10.1038/ncomms4298, 2014.

825 Guan, M., Wright, N. G., and Sleigh, P. A.: Multimode morphodynamic model for sediment-laden flows and geomorphic
826 impacts, *Journal of Hydraulic Engineering*, 141(6), doi:10.1061/(ASCE)HY.1943-7900.0000997, 2015

827 Guo, Q., Hu, C., and Takeuchi, K.: Numerical modeling of hyper-concentrated sediment transport in the lower Yellow River,
828 *Journal of Hydraulic Research*, 46(5), 659-667, doi:10.3826/jhr.2008.3009, 2008.

829 Harten, A., Lax, P. D., and van Leer, B.: On upstream differencing and Godunov-type schemes for hyperbolic conservation
830 laws, *SIAM Review*, 25(1), 35-61, 1983.

831 He, L., Duan, J. G., Wang G., and Fu, X.: Numerical simulation of unsteady hyperconcentrated sediment-laden flow in the
832 Yellow River, *Journal of Hydraulic Engineering*, 138(11), 958-969, doi:10.1061/(ASCE)HY.1943-7900.0000599,
833 2012.

834 Hirano, M.: On riverbed variation with armoring, *Proc. Jpn. Soc. Civ. Eng.*, 195, 55-65, 1971, (in Japanese).

835 Hoey, T. B. and Ferguson, R.: Numerical simulation of downstream fining by selective transport in gravel bed rivers: Model
836 development and illustration, *Water Resour. Res.*, 30(7), 2251-2260, doi:10.1029/94WR00556, 1994.

837 Ma, H., Nittrouer, J. A., Naito, K., Fu, X., Zhang, Y., Moodie A. J., Wang, Y., Wu, B., and Parker, G.: The exceptional
838 sediment load of fine-grained dispersal systems: Example of the Yellow River, China, *Science Advances*, 3(5),
839 e1603114, doi:10.1126/sciadv.1603114, 2017.

840 Mart ń-Vide, J. P., Amarilla, M., and Z ́arate, F. J.: Collapse of the Pilcomayo River, *Geomorphology*, 205(15), 155-163, 2014.

- 841 Meyer-Peter, E. and Müller, R.: Formulas for bed-load transport, in Proceeding of the 2nd IAHR Meeting, International
842 Association for Hydraulic Research, 7-9 June 1948, Stockholm, Sweden, 39-64, 1948.
- 843 Milliman, J. D. and Meade, R. H.: World-wide delivery of river sediment to the oceans, *The Journal of Geology*, 91(1), 1-21,
844 1983.
- 845 Minh Duc, B. and Rodi, W.: Numerical simulation of contraction scour in an open laboratory channel, *Journal of Hydraulic
846 Engineering*, 134(4), 367-377, doi:10.1061/(ASCE)0733-9429(2008)134:4(367), 2008.
- 847 Naito, K., Ma, H., Nittrouer, J., Zhang, Y., Wu, B., Wang, Y., and Parker, G.: Extended Engelund-Hansen type sediment
848 transport relation for mixtures based on the sand-silt-bed Lower Yellow River, China, *Journal of Hydraulic Research*,
849 accepted subject to revision, 2018.
- 850 National Research Council: *River Science at the U.S. Geological Survey*. Washington, DC: The National Academies Press,
851 available at: <https://doi.org/10.17226/11773>, 2007.
- 852 Ni, J. R., Zhang, H. W., Xue, A., Wieprecht, S., and Borthwick, A. G. L.: Modeling of hyperconcentrated sediment-laden
853 floods in Lower Yellow River, *Journal of Hydraulic Engineering*, 130(10), 1025-1032, 2004.
- 854 Paola, C., Heller, P. L., and Angevine, C. L.: The large-scale dynamics of grain-size variation in alluvial basins, I: Theory,
855 *Basin Research*, 4, 73-90, 1992.
- 856 Parker, G.: *1D Sediment Transport Morphodynamics with Applications to Rivers and Turbidity Currents*, available at:
857 http://hydrolab.illinois.edu/people/parkerg//morphodynamics_e-book.htm, 2004.
- 858 Parker, G., Paola, C., and Leclair, S.: Probabilistic Exner sediment continuity equation for mixtures with no active layer,
859 *Journal of Hydraulic Engineering*, 126(11), 818-826, 2000.
- 860 Phillips, B. C. and Sutherland A. J.: Spatial lag effects in bedload sediment transport, *Journal of Hydraulic Research*, 27(1),
861 115-133, doi:10.1080/00221688909499247, 1989.
- 862 Stecca, G., Siviglia, A., and Blom, A.: Mathematical analysis of the Saint-Venant-Hirano model for mixed-sediment
863 morphodynamics, *Water Resources Research*, 50, 7563-7589, doi:10.1002/2014WR015251, 2014.
- 864 Stecca, G., Siviglia, A., and Blom, A.: An accurate numerical solution to the Saint-Venant-Hirano model for mixed-sediment
865 morphodynamics in rivers, *Advances in Water Resources*, 93(Part A), 39-61, doi:10.1016/j.advwatres.2015.05.022,
866 2016.
- 867 Toro, E. F.: *Shock-capturing methods for free-surface shallow flows*, John Wiley, 2001
- 868 Toro-Escobar, C. M., Parker, G., and Paola, C.: Transfer function for the deposition of poorly sorted gravel in response to
869 streambed aggradation, *Journal of Hydraulic Research*, 34(1), 35-53, doi:10.1080/00221689609498763, 1996.
- 870 Tsujimoto, T.: A probabilistic model of sediment transport processes and its application for erodible-bed problems, Ph.D.
871 thesis, Kyoto University, Kyoto, Japan, 1978, (in Japanese).
- 872 Van der Scheer, P., Ribberink, J. S., and Blom, A.: Transport formulas for graded sediment; Behaviour of transport formulas
873 and verification with data. Research Report 2002R-002, Civil Engineering, University of Twente, Netherlands, 2002.

874 Viparelli, E., Sequeiros, O. E., Cantelli, A., Wilcock, P. R., and Parker, G.: River morphodynamics with creation/consumption
875 of grain size stratigraphy 2: numerical model, *Journal of Hydraulic Research*, 48(6), 727-741,
876 doi:10.1080/00221686.2010.526759, 2010.

877 Wang, S., Fu, B., Piao, S., Lü Y., Ciais, P., Feng, X., and Wang, Y.: Reduced sediment transport in the Yellow River due to
878 anthropogenic changes, *Nature Geoscience*, 9, 38-41, doi:10.1038/ngeo2602, 2016.

879 Wu, W. and Wang, S. S. Y.: One-dimensional modeling of dam-break flow over movable beds. *Journal of Hydraulic*
880 *Engineering*, 133(1), 48-58, 2007.

881 Wu, W. and Wang, S. S. Y.: One-dimensional explicit finite-volume model for sediment transport, *Journal of Hydraulic*
882 *Research*, 46(1), 87-98, 2008.

883 Wu, W., Vieira, D. A., and Wang, S. S. Y.: A 1-D numerical model for nonuniform sediment transport under unsteady flows
884 in channel networks, *Journal of Hydraulic Engineering*, 130(9), 914-923, doi:10.1061/(ASCE)0733-
885 9429(2004)130:9(914), 2004.

886 Xu, J.: Erosion caused by hyperconcentrated flow on the Loess Plateau of China, *Catena*, 36(1999), 1-19, 1999.

887 Zhang, H., Huang, Y., and Zhao, L: A mathematical model for unsteady sediment transport in the Lower Yellow River,
888 *International Journal of Sediment Research*, 16(2), 150-158, 2001.

889 Zhang, S. and Duan, J. G.: 1D finite volume model of unsteady flow over mobile bed, *Journal of Hydrology*, 405, 57-68,
890 doi:10.1016/j.jhydrol.2011.05.010, 2011.

891 Zhang, S., Duan, J. G., and Strelkoff T. S.: Grain-scale nonequilibrium sediment-transport model for unsteady flow, *Journal*
892 *of Hydraulic Engineering*, 139(1), 22-36, doi:10.1061/(ASCE)HY.1943-7900.0000645, 2013.